

# Single blade installation with a floating monohull vessel

---

Establishing the operational limits while using dynamic controlled taglines

European Wind Energy Master – Offshore Engineering

A.L. Slootweg





# Single blade installation with a floating monohull crane vessel

Establishing the operational limits while using  
dynamic controlled taglines

by

**A.L. Slootweg**

This report is submitted as fulfilment of the course OE54030EWEM MSc Thesis  
and partial fulfilment of the requirements to obtain the degree of:

Master of Science in Offshore & Dredging Engineering at Delft University of Technology  
&  
Master of Science in Wind Energy Technology at Norwegian University of Science and Technology  
under the [European Wind Energy Master](#) programme.

To be defended publicly on September 30, 2021 9.30 AM

Officially handed in on September 16, 2021

Faculty of Mechanical, Maritime and Materials Engineering, Delft University of Technology

Faculty of Marine Technology, Norwegian University of Science and Technology

Student number:	4431995 (TU Delft), 537166 (NTNU)
E-mail:	<a href="mailto:laura.slootweg@gmail.com">laura.slootweg@gmail.com</a>
Project duration:	January, 2021 – September, 2021
Supervisors:	S.A. Miedema, Ph.D. TU Delft, chairman P. Naaijen, Ph.D. TU Delft, supervisor Prof. Z. Gao, NTNU, supervisor E. Vlasveld, M.Sc. GustoMSC, supervisor

*This thesis is confidential and cannot be made public until September 30, 2023*



# Acknowledgement

Writing this thesis has been a truly rewarding, educating, and inspiring experience for me, but I would like to acknowledge that this would not have been possible without the guidance and support of several persons.

Firstly, I would like to thank my supervisor Ebert Vlasveld for meeting with me every week to discuss the project. You helped me a lot during the project and often made me zoom-out to see the bigger picture. Also, I would like to thank my supervisors from the NTNU and TU Delft, Zhen Gao, Peter Naaijen, and Sape Miedema. This thesis would not have been possible without their supervision, guidance, and technical expertise. Moreover, I would also like to express my gratitude for your understanding, patience, and kindness during the unanticipated adversities which arose during the course of the semester.

During my thesis project I spend a lot of time at the GustoMSC office. Here, I made friends and got a lot of support from colleagues of varying departments. I would like to thank all of the colleagues who helped me and brought new ideas to the table during the project, this brought the thesis to a new level. Especially I would like to thank Koen Baron for teaching me everything about feedback control with much patience. And thanks to my fellow graduates Niels, Calvin, and Nina, for sparring about our projects and all the table tennis matches.

During the thesis there were many ups and downs, which I certainly did not go through alone. My roommates Yarden and Eefje had to deal with my everyday stress, struggle, and victory. Thank you for being there, thank you for caring for me during the hard times, and cheering me up after a bad day. Last, I would like to thank Alex for being able to make me laugh at any time of the day, in any kind of mood. You are a joy.

Last and most importantly, my deepest gratitude, appreciation, and love extends to my family. To my sister and brother, Emilie and Wouter, for keeping me humble and making me the person I am today. And to my parents, Nico and Nathalie, who made this education possible for me, and whom extended their never-ending love and support to me my entire life. I have always striven, and will keep striving, to make you proud.



# Abstract

Larger wind turbines are being developed to fill the growing demand for green energy. Wind turbines that need to be installed in the next decade will reach a capacity of 15 MW, with an approximate rotor diameter of 240 meters. The currently used wind turbine installation vessels cannot install these larger wind turbines; hence, investments need to be made. An opportunity arises from the oil and gas industry: investments in this industry are decreasing. Thus, the floating monohull fleet working in this industry will need repurposing in the upcoming decade.

In this thesis, the operational limit of a single blade installation with a floating monohull crane vessel is sought. An installation method is proposed where taglines are used to compensate vessel motions and wind loads on the blade. Motion compensation with taglines is a technology that is already being used in the industry, which makes it attractive to contractors who are hesitant to use new technologies. The proposed installation concept uses three different compensation systems, allowing the blade motions to be decoupled and controlled separately. One of the compensation systems is selected and investigated in more detail in this research. The selected compensation system compensates for the blade motion in  $y$ - and yaw-direction with two dynamically controlled taglines horizontally attached from the blade to the crane boom.

The operational limit is determined for the final installation stage, the mating phase between the blade and the hub. The alignment of the blade and the hub is modeled in frequency- and time-domain. From these models, it can be concluded that the control system can limit the  $y$ -motions at the blade root below typically accepted motion limits, when the wave direction is limited to an interval of  $150\text{-}210^\circ$ , for a sea state up to a wave height of  $H_s = 5.6$  m and wave peak period  $T_p$  of 10 s. However, this is only true when the pre-displacement of the blade towards the crane boom is larger than the maximum crane tip displacement.

Based on these preliminary findings, it seems that floating installation of turbine blades could be feasible with proper tagline control. Further investigation, involving dynamic control in all degrees of freedom, is therefore recommended.





# List of Figures

1.0.1 Capacity and turbine size growth over the past decades and future expectations [1] . . . . .	3
2.1.3 Single blade installation methods . . . . .	7
2.1.1 Installation methods [2] . . . . .	8
2.1.2 Connection of a turbine blade to the hub (figure from GustoMSC) . . . . .	8
2.1.4 Bunny-ears installation [3] . . . . .	10
2.1.5 Three pre-installed blades [4] . . . . .	10
2.1.6 Arcadis installing the RNA using a dummy tower [5] . . . . .	12
2.1.7 Vertical installation frame by TWD [6] . . . . .	12
2.1.8 Climbing crane by Lagerwey [7] . . . . .	12
2.3.1 Wave direction in respect to the vessel . . . . .	15
2.3.2 Illustration of the weather window (DNV-OS-H101 [8]) . . . . .	16
2.4.1 Top view of installation method . . . . .	18
2.4.2 Frond view of installation method . . . . .	18
2.5.1 Distance between hub center and blade root center $d_{hb}$ . . . . .	19
3.1.1 Side and front view of the installation vessel with blade [9] . . . . .	22
3.1.2 The top view of the installation vessel with blade . . . . .	22
3.2.1 Compensation systems in x-, z-, and $\theta$ -direction . . . . .	23
3.2.2 Top and frond view of vessel with compensation in y- and $\psi$ -direction . . . . .	24
3.2.3 Situation 1 (top): Forces on the blade in y-direction without pretension. Situation 2 (bottom): Forces on the blade in y-direction with pretension. . . . .	25
3.2.4 Schematic illustration of side-view of the winch system . . . . .	26
3.4.1 Pendulum model with moving base and a horizontally applied tagline force . . . . .	28
3.5.1 Illustration of the connection between time and frequency domain representation of a long crested short term sea state [10] . . . . .	31
4.1.1 Basic feedback control system . . . . .	36
4.1.2 PID-controller . . . . .	36
4.3.1 Force spectrum of wave and wind induced forces on the blade . . . . .	40
4.3.2 Moment spectrum around the blade z-axis due to wind and wave loading . . . . .	42
5.2.1 Most probable maximum displacement of blade root in y-direction with and without feedback controlled taglines (30-minute reference period) . . . . .	50

5.2.2 Most probable maximum blade root displacement $y_{br}$ per wind and wave condition with and without feedback controlled taglines (30-minute ref. period) . . . . .	51
5.2.3 $y_{br,mpm}$ per wave direction, wave peak period, and with a mean wind speed of 10 m/s (30-minute ref. period) . . . . .	52
6.3.1 RAOs determined in frequency domain and by time simulations of the 6DOF of the vessel with a wave heading of $180^\circ$ . . . . .	57
6.3.2 RAOs determined in frequency domain and by time simulations of the 6DOF of the vessel with a wave heading of $165^\circ$ . . . . .	57
6.3.3 Spectrum of wind induced moment on the blade with a mean wind speed of 6 m/s . . . . .	58
6.6.1 Maximum y-displacements per sea state . . . . .	61
6.6.2 Maximum y-displacement of blade root per mean wind speed . . . . .	62
6.6.3 Results for maximum blade root y-displacement with simultaneously simulated wind and wave loads, the mean wind speed is 10 m/s, the wave direction is $\psi=150^\circ$ , the results plotted per peak period of the wave excitation spectra . . . . .	63
7.1.1 Y-displacement of blade root in frequency (f) and time (t) domain due to wave loads	66
7.1.2 Y-displacement of blade root in frequency- (f) and time- (t) domain due to wind loads, per mean wind speed between 2-10 m/s . . . . .	67
7.1.3 Y-displacement of blade root in frequency (f) and time (t) domain due to wind with $V_{10} = 10$ m/s, and varying wave loads . . . . .	67
B.0.1 Side view of GustoMSC Ensyst XL . . . . .	84
B.0.2 Top view of GustoMSC Ensyst XL . . . . .	85
C.0.1 RAO for 6 degrees of freedom for a loading condition with a low draft and a high GM	88
D.1.1 The open loop $L$ function, and the sensitivity function $S$ for compensation in y-direction	90
D.1.2 The closed loop function $T$ , for compensation in y-direction . . . . .	91
D.1.3 Nyquist plot for $\psi$ -compensation system . . . . .	91
D.2.1 The open loop $L$ function, and the sensitivity function $S$ for compensation in $\psi$ -direction . . . . .	92
D.2.3 Nyquist plot for y-compensation system . . . . .	93
D.2.2 The closed loop function $T$ , for compensation in $\psi$ -direction . . . . .	93
D.3.1 The dimensionless load sensitivity function for y-direction . . . . .	94
D.3.2 The dimensionless load sensitivity function for $\psi$ -direction . . . . .	94

# List of Tables

- 2.2.1 MPM displacement in x-, y-, and z-direction for  $H_s = 2$  m,  $T_p = 8$  s, and a wave heading of  $180^\circ \pm 15^\circ$ , for four loading conditions . . . . . 14
- 4.3.1 Mean force in blade y-direction due to a mean wind speed of 2-10 m/s . . . . . 40
- 4.3.2 Mean moment around blade z-axis due to a mean wind speed of 2-10 m/s . . . . . 42
- 4.4.1 PID-controller parameters for y-compensation . . . . . 44
- 4.4.2 PID-controller parameters for  $\psi$ -compensation . . . . . 44
- 6.3.1 Analytical and load case model results of static heel and decay test . . . . . 55
- 6.6.1 Maximum blade root displacements for two different sets of environmental conditions with ten different randomness seeds . . . . . 63
- 6.6.2 Needed winch capacity . . . . . 64
- A.1.1 Vessel Properties from WAMIT data (\*:from water line, midship, on the stern) . . . 79
- A.2.1 Blade properties [11] . . . . . 80
- A.3.1 Nodes of IEA 15MW reference turbine blade [11] . . . . . 81
- A.4.1 Segments of IEA 15 MW reference turbine blade [11] . . . . . 82



# Contents

<b>1</b>	<b>Introduction</b>	<b>3</b>
1.1	Problem description . . . . .	4
1.2	Research objective . . . . .	5
1.3	Report outline . . . . .	5
<b>2</b>	<b>Concept design of lifting operation</b>	<b>7</b>
2.1	Methods for rotor-nacelle assembly installation . . . . .	7
2.2	Equipment . . . . .	14
2.3	Environmental conditions . . . . .	15
2.4	Concept selection . . . . .	17
2.5	Motion criteria during the critical phase . . . . .	17
2.6	Conclusion . . . . .	20
<b>3</b>	<b>Modeling of lifting arrangement</b>	<b>21</b>
3.1	Definition of degrees of freedom . . . . .	21
3.2	The compensation system concept . . . . .	22
3.3	Assumptions . . . . .	27
3.4	Equations of motion . . . . .	28
3.5	Modeling strategy . . . . .	30
3.6	Conclusion . . . . .	33
<b>4</b>	<b>Tagline control</b>	<b>35</b>
4.1	Feedback control . . . . .	35
4.2	Plant transfer functions . . . . .	37
4.3	Disturbance loads . . . . .	38
4.4	Controller parameters . . . . .	42
4.5	Conclusion . . . . .	45
<b>5</b>	<b>Frequency domain model</b>	<b>47</b>
5.1	Model description . . . . .	47
5.2	Frequency domain results . . . . .	50

<b>6</b>	<b>Time domain model</b>	<b>53</b>
6.1	General theory behind aNySIM . . . . .	53
6.2	Overview aNySIM model . . . . .	54
6.3	Model verification . . . . .	55
6.4	Tagline modeling . . . . .	58
6.5	Model description . . . . .	59
6.6	Results time domain simulation . . . . .	60
<b>7</b>	<b>Analysis of frequency and time domain results</b>	<b>65</b>
7.1	Analysis and comparison of results . . . . .	65
7.2	Observed differences discussion . . . . .	68
<b>8</b>	<b>Discussion</b>	<b>71</b>
<b>9</b>	<b>Conclusion</b>	<b>73</b>
<b>10</b>	<b>Recommendations</b>	<b>75</b>
<b>A</b>	<b>Vessel and Blade data</b>	<b>79</b>
A.1	Vessel data . . . . .	79
A.2	Blade data . . . . .	80
A.3	Blade nodes . . . . .	81
A.4	Blade segments . . . . .	82
<b>B</b>	<b>EnsysXL drawings</b>	<b>83</b>
<b>C</b>	<b>RAO - low draft and high GM</b>	<b>87</b>
<b>D</b>	<b>Bode and Nyquist</b>	<b>89</b>
D.1	Y-system . . . . .	90
D.2	$\psi$ -compensation . . . . .	92
D.3	Load sensitivity functions . . . . .	94



# 1 | Introduction

In the Paris Agreement of 2015, a goal was set: the global temperature rise should stay below  $2^\circ$ , preferably  $1.5^\circ$ . To achieve this, the European Commission estimates that we will need 450GW of installed offshore wind power by 2050 [12]. In 2019 there was an installed capacity of 22GW, which means that around 53,500 8-MW offshore wind turbines (OWT) must be installed in the upcoming 30 years. The capacity of OWTs keeps increasing; see Figure 1.0.1. If the wind turbine size is increased, a smaller quantity of turbines needs to be installed to achieve the goals for 2050. However, new challenges arise with the increasing capacity. To obtain the extra power, the rotor radius, and hub height increase in size. The increasing heights and masses bring challenges for the transportation and installation of the OWTs.

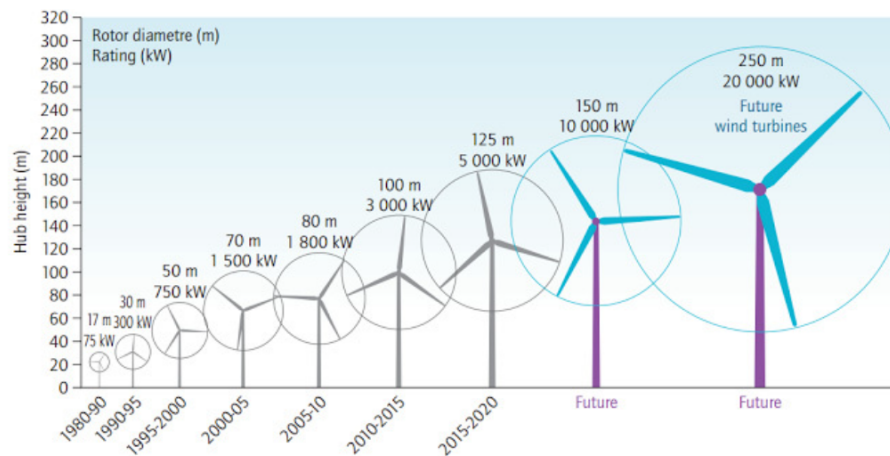


Figure 1.0.1: Capacity and turbine size growth over the past decades and future expectations [1]

GustoMSC is a design and engineering consultancy for mobile offshore units and equipment. GustoMSC has a significant market share in the engineering and design of jack-up vessels. Currently, many OWTs are installed using jack-up vessels that the company designed. Since the market is growing and wind turbine sizes are increasing, larger wind turbine installation vessels will be required. To meet the future demands, GustoMSC is exploring new methods for OWT installation by looking into installation possibilities with floating vessels.

Currently, all operable offshore wind turbine installation vessels (OWTIV) are jack-up vessels. These jack-up vessels are expensive vessels per tonnage of variable load in comparison with floating



monohull vessels. Due to the increasing dimensions of the future turbines, and the increasing installation depths, significant investments are required to acquire higher capacity jack-up vessels. Since significant investments need to be made, finding a more economically feasible solution might benefit the sector. An opportunity arises from the Oil and Gas (O&G) industry. Due to decreasing investments in the O&G sector in recent years [13], the existing fleet needs repurposing in the upcoming decades. Should installation of wind turbine blades with floating vessels prove to be feasible, the investments could be directed to repurposing the existing O&G fleet to floating wind turbine installation vessels.

At present, several installation methods have been used to install the rotor nacelle assembly (RNA). In industry, single blade installation is the most frequently used method to install wind turbine blades. The blades are installed one by one instead of installing several blades in one lift. Having to transport single blades makes the transportation of the blades practical and the lifting and control of the blade during the lifting operation easier and thus safer. The main benefit of using single-blade installation is that the blades can be detached from the hub for maintenance when needed, while the hub and the other blades can stay on the tower.

This thesis considers the single blade installation of a 15MW wind turbine blade with a monohull crane vessel. The wave-induced vessel motions will be problematic during the installation of the blade, especially during the mating phase, when the blade root is connected to the wind turbine hub. In this final phase of installation, the motions of the blade need to be very small to ensure a safe installation.

## 1.1 Problem description

At present, taglines are used during the installation of wind turbine blades to keep the blade stable in space and compensate for wind-induced blade motions. The benefit of using tagline systems is that the system is relatively cheap compared to other stabilizing systems, and the system can be used on every vessel. Additionally, contractors have a significant say in the installation method used during the operation, and they are often hesitant to use new installation technologies due to unknown risks.

Wind turbines are not yet being installed with monohull vessels due to their sensitivity to wave loads. The combination of the wave-induced vessel motions and the large operation height results in large motions that need to be compensated during the installation. To find the feasibility of installing wind turbine blades while using a monohull crane vessel, an installation method must be found that compensates for the wave-induced motions while preferably using known compensation systems like taglines.

## 1.2 Research objective

GustoMSC is a pioneer in offshore engineering. Therefore, they want to investigate the feasibility of installing OWTs with floating monohull crane vessels. New techniques are expected to be necessary to install the 15MW wind turbines with the monohull vessel due to its sensitivity to wave loads. A solution needs to be found to compensate for the vessel motions to guarantee safety during installation.

This project aims to find the operational limits of single-blade installation with a monohull crane vessel while reducing the blade motions with actively controlled taglines. The main research question is as follows:

“How can the blade motions during a single blade installation with a floating monohull crane vessel be reduced with a dynamic tagline system, and what would the operational limits of the installation be?”

Several sub-questions need to be answered to find an adequate answer to the main research question:

1. What is the optimal configuration of the taglines and other control elements for the stability of the blade during installation?
2. On which critical phase of the installation should the operational limits be based?
3. What are the motion boundaries of the blade for safe blade installation during the critical phase?
4. Which factors will influence the blade motions, and to what extent should they be considered in a numerical model?
5. What is the most appropriate numerical modeling strategy that yields sufficiently accurate results regarding the blade motion envelope?

## 1.3 Report outline

Chapter 2 aims to give a summary of the currently used installation methods and to introduce the lifting concept that is used in this research. The lifting concept for this research is described by specifying the vessel and blade data used and describing the blade installation method with a monohull vessel. Chapter 3 focuses on the modeling of the critical phase of the installation. The compensation systems are discussed in more detail, the main assumptions are stated, and the modeling strategy is discussed. In Chapter 4, the control system for the taglines is discussed. In Chapter 5, the frequency domain model set-up is described, and the operational limits according to this model are given. In the next chapter, a non-linearity is introduced. A time domain model is needed to include this in the system. In Chapter 6, the time domain model is described and verified. The chapter concludes with the results from the time domain model. The results of the frequency and time domain calculations are compared and discussed in Chapter 7. A discussion about the results is given in Chapter 8. The report ends with the conclusions and recommendations following from this project in Chapters 9 and 10.



## 2 | Concept design of lifting operation

### 2.1 Methods for rotor-nacelle assembly installation

There are several ways of installing wind turbine blades and nacelle. In this section, the existing installation methods are named, and the advantages and disadvantages are discussed.

The main difference between the methods is the number of lifts needed to install the tower and rotor nacelle assembly (RNA). An offshore wind turbine can be divided into multiple parts for installation; the components that are used in practice are shown in Figure 2.1.1.

#### 2.1.1 Single blade installation

In the first two methods in Figure 2.1.1, every blade is installed separately after installing the tower in one or two lifts and installing the nacelle and hub; this is called single blade installation. The installation is done by first lifting the nacelle and connecting the tower in one or more pieces to the transition piece. After that, the nacelle is lifted and installed on top of the tower. The installation is finalized by lifting every blade and connecting them to the hub one by one. A blade is connected using pins, as is shown in Figure 2.1.2. Generally, two slightly longer pins guide the blade into the hub, where the other pins fall into place, then the blade can be connected safely to the hub.

In order to install every blade with the same procedure, the rotor must turn  $120^\circ$ , so the connection point of the hub is at the same location. There are three ways to install single blades: vertical, horizontal, and diagonal. The three different methods are displayed in Figure 2.1.3.



Figure 2.1.3: Single blade installation methods


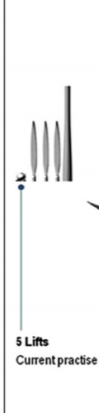
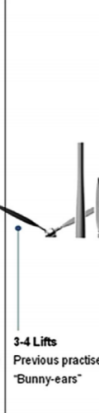



Number of Lift						
	6 Lifts Current practise	5 Lifts Current practise	3-4 Lifts Previous practise "Bunny-ears"	3-4 Lifts Current practise "Star Assy"	2 Lifts Proposed	Single lift Proposed
Installation method	1	2	3	4	5	6

Figure 2.1.1: Installation methods [2]



Figure 2.1.2: Connection of a turbine blade to the hub (figure from GustoMSC)

Currently, the OWT blades are mainly installed horizontally, which has two main reasons. One is that when a blade is picked up horizontally, the blade can be lifted by the pickup tool while gravity works in its favor, and thus less force needs to be added to hold the blade in place. The blade has to be picked up and held in position using friction between the blade and the pickup tool with vertical or diagonal installation. The blade must be strong enough to withstand these specific loads, and the pickup tool needs to be more advanced. Another reason horizontal installation is used more often is that the blade is better manageable, sway and yaw movements of the blade can be controlled using taglines. For diagonal installation, the control over the blade position is more complex because the blade needs to be under the right angle for installation. With vertical installation, the blade needs to be lifted eccentrically to avoid the cable coming into contact with the hub. The blade and pickup tool tend to rotate around its center; however, this motion can be controlled by using tuggerlines from the deck [17].

For single blade installation the following advantages and disadvantages must be considered:

Wind-induced loads	The wind-induced loads on one blade during installation are easier to predict than the wind-induced loads on a structure with several blades attached.
Mass	The weight of one blade is small in comparison with other methods.
Transportation	Transportation can be done very efficiently because a scaffolding can be used for the blades.
Maintenance	When maintenance needs to be done on a blade, the blade can be disconnected easily since they were installed one by one.
Installation speed	According to Ahn’s research assessment on different offshore installation vessels, the vessels that have installed with the single blade installation method were the vessels with the highest turbines per day rate in the past [2].
Lifting amount	Single blade installation requires the largest amount of lifts needed to install one turbine.
Electricity in hub	Turning the hub to position it for the next blade costs electricity, getting the power to the top of the turbine is not easy.

### 2.1.2 Bunny-ears installation

A second method is to connect two of the blades to the rotor onshore and installing the nacelle and two blades in one lift. Figure 2.1.4 shows a “bunny-ears” construction being transported to the installation site. For the “bunny-ears” installation method, the following advantages and disadvantages must be considered:

Lifting amount	This method requires one or two lifts less than with single lift installation.
Electricity in hub	There is no power needed in the top of the wind turbine to rotate the hub.
Transportation	Is less efficient, resulting in the ship having to go back to the port to collect new wind turbine parts more often.
Lifting complexity	The lifting operation is more complex than a single blade installation because the mass in the crane increases, and two blades are subject to wind loads.
Two different installation methods	The last blade needs to be up-ended and installed vertically, so two different installation procedures are needed to install one turbine.



Figure 2.1.4: Bunny-ears installation [3]



Figure 2.1.5: Three pre-installed blades [4]

### 2.1.3 Three pre-installed blades

The fourth method stated in Figure 2.1.1 consists of the installation of a tower, nacelle, and a rotor hub with three pre-installed blades. All the blades are connected to the hub onshore. On location, the tower and nacelle are installed, after which the hub with its three blades is installed in one lift. In Figure 2.1.5 an installation of the hub with three blades is displayed. For the installation with three pre-installed turbine blades, the following advantages and disadvantages must be considered:

Lifting amount	This method requires only one lift to install the hub and all blades.
Electricity in hub	There is no power needed in the top of the wind turbine to rotate the hub.
Transportation	Is less efficient, resulting in the ship having to go back to the port to collect new wind turbine parts more often.
Logistics	Port logistics are more complex due to the large size and shape of the structure.
Lifting complexity	The lifting procedure is complex because the hub-blade structure needs to be lifted into the air, then rotated 90°, and then installed.
Wind loads	During the installation, the wind-induced forces on the hub-blade structure are hard to predict.
Maintenance	When a blade needs to be taken off of the turbine for maintenance, there is a probability that the entire hub needs to be taken off and transported to shore instead of just one blade.

### 2.1.4 Single lift installation

The last method in Figure 2.1.1 is to pre-assemble the entire OWT onshore and install the wind turbine in one lift. For the installation with three pre-installed turbine blades the following advantages and disadvantages must be considered:

Lifting amount	This method requires only one lift to complete the entire installation on site.
Experience	It has not been done many times before; therefore there is less historical data to base the operation on.
Transportation	Transportation to the site is not an easy procedure. A sheer leg crane vessel can transport one OWT. If multiple OWTs are wished to be transported, a new vessel needs to be designed to transport the OWTs.
Structural integrity	The entire structure of the OWT must be suitable for such an operation, especially the connection between the tower and the RNA must be checked.

### 2.1.5 Alternative installation methods

There are many disadvantages to each method. Therefore, new installation methods are still being developed. In this subsection, several developments are discussed.

#### Floating installation with a dummy tower - Heerema

The first floating installation is scheduled to be done by Heerema. They plan to assemble the RNA on a dummy tower onboard, after which the total RNA is lifted and installed on the wind turbine tower. The procedure is shown in Figure 2.1.6. This has the following advantages, and disadvantages should be considered:

Transportation	Can be done relatively efficiently because the blades can be transported with a blade rack.
Electricity in hub	The power needed to turn the hub can be connected easier using the dummy tower.
Ship motions	The dummy tower moves with the ship. The installation of the RNA is easier to do since the crane and optional tagline system are subject to the same ship motion.
Ship motions	Only one lift has to be done to the real OWT tower
Accessibility during the installation	The installation of the blades on the deck gives the advantage that all is easily accessed
Maintenance	When a blade needs to be exchanged for maintenance or repair, the nacelle has to come off entirely instead of only one blade.
Collegian risk	The crane and dummy tower must have a sufficient distance between each other to minimize the chance of collegian between the RNA on the dummy tower and the crane.
Control during final lift	Controlling the movements of the RNA during the lift to the tower is hard and complex because taglines cannot be connected to the blades, which makes it hard to gain momentum with the taglines, and the wind induced loads on the structure is hard to predict.



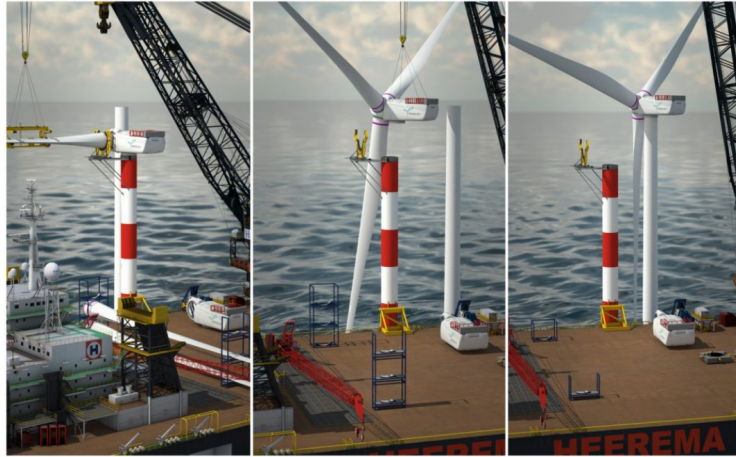


Figure 2.1.6: Arcadis installing the RNA using a dummy tower [5]

### Vertical installation frame - TWD

Temporary Work Design has developed a frame to install wind turbine blades using a frame to guide the blade vertically to the hub. The frame during installation is shown in Figure 2.1.7. The main goal of this method is to install blades when the weather is not ideal. The system would be equipped with a dynamic stabilizing system to steady the blade. This design has several objections. The frame can only install blades, so a vessel is needed to install the nacelle and hub, which means a lifting procedure is needed either way. To use this robust method, electricity power is needed in the hub to rotate the hub, which will make the installation more complex. When the environmental loads increase, the wind turbine motions will also increase. The tower will have significant motions, especially when two blades are installed and the third blade is installed. The dynamic compensation system needs to be able to compensate for those movements.



Figure 2.1.7: Vertical installation frame by TWD [6]



Figure 2.1.8: Climbing crane by Lagerwey [7]

### **Climbing crane - Lagerwey**

The climbing crane by Lagerwey is a crane that moves upwards and installs the wind turbine piece-by-piece. The final blade installation is shown in Figure 2.1.8. This could be an excellent alternative to install wind turbine blades with a mechanism attached to the wind turbine itself. However, the concept is not yet proven in an offshore environment.

#### **2.1.6 Lifting operation for this research**

For OWT blade installation, the single blade installation method is most frequently used in industry nowadays. The main advantage of this method, compared to the other installation methods, is that it requires the least complex lifting operation, the transportation of the parts is considerably easy, and maintenance to a blade can be done without uninstalling the entire hub or nacelle. The downside of single blade installation compared to other lifting methods is that more lifts are needed to complete the entire installation. Since contractors are reluctant to use new installation methods, installation methods that are already being used are preferred. Since the installation of OWT blades with a monohull crane vessel is an operation that has never been performed before, the complexity of the operation is an essential factor. Hence, single blade installation is the installation method that seems to be the best fit for blade installation with a floating monohull crane vessel.

## 2.2 Equipment

The single blade installation of this project is done with a large monohull crane vessel and a 15MW wind turbine blade. In this section, the vessel specifications are given, and the blade characteristics are described.

### 2.2.1 Vessel specification

Due to decreasing investments, the monohull fleet currently working for the oil and gas industry will need repurposing in the next decade. This research investigates if a monohull crane vessel can be used to install OWTs, and thus if these O&G vessels can be repurposed into installing wind turbines. A specific monohull crane vessel must be selected. In a constant sea state, the wave induced motions on a ship decrease when ship size increases. Hence, the installation is more likely to be feasible with a larger vessel. To start with research on wind turbine blade installation with a floating monohull vessel, the GustoMSC Enslys XL is selected. The Enslys XL is a 280 m long, 55 m wide monohull crane vessel shown in Appendix B. Further specifications are given in Appendix A. When the single blade installation proves to be feasible with this large vessel, further research can be done to explore the possibilities for installation with smaller vessels.

The loading condition of the vessel affects the wave response of the vessel. Different loading conditions must be evaluated to determine which loading condition will be used for the first calculations. The least favorable loading condition will be used in the initial calculations to get a conservative but realistic result. In the literature review previous to this report [18], a model is used to determine the most probable maximum (MPM) (of a 3-hour reference period) displacements of the crane tip in a sea state with a significant wave height  $H_s = 2.0$  m and a peak period  $T_p$  of 4-10 s. This model can be used to determine the MPM displacements per loading condition. The four loading conditions creating the operational envelope are a combination of a high or low GM and draft. For each loading condition the MPM displacement in x-, y-, and z-direction with a sea state with  $H_s = 2$  m,  $T_p = 8$ , and a wave heading of  $180^\circ \pm 15^\circ$  is given in Table 2.2.1. From this data, it can be concluded that the loading condition with a low draft and a high GM is the most conservative. Hence, this is the loading condition that will be used in this research.

Table 2.2.1: MPM displacement in x-, y-, and z-direction for  $H_s = 2$  m,  $T_p = 8$  s, and a wave heading of  $180^\circ \pm 15^\circ$ , for four loading conditions

Loading condition	MPM x-displacement [m]	MPM y-displacement [m]	MPM z-displacement [m]
High draft, high GM	1.06	0.16	0.26
High draft, low GM	0.88	0.08	0.23
Low draft, high GM	1.42	0.38	0.4
Low draft, low GM	1.24	0.09	0.33

### 2.2.2 Blade specifications

Currently, wind turbines of approximately 8MW are being installed. However, companies like Siemens Gamesa and General Electrics are developing future offshore wind turbines of 12 to 15 MW. This research focuses on the installation of future wind turbines. Hence, the IEA 15MW

reference wind turbine is used. The IEA 15MW reference wind turbine blade is 117 meters long and weighs about 65 tons. Further general information of the wind turbine blade is added in Appendix A.2, the blade node and segment data is given in Appendix A.3 and A.4.

## 2.3 Environmental conditions

An offshore operation is usually weather restricted, which means that the operation can be executed up to specific environmental conditions. The environmental conditions of an offshore operation can generally be divided into wind and wave conditions. These conditions are often described with the characteristics of a power spectrum. For this project, the operational limits are sought for the installation of wind turbine blades with a floating vessel. To direct the research, and environmental envelope is formulated. The environmental envelope reaches up to the operational limits of wind turbine blade installation with a jack-up vessel. First, the wave conditions of the environmental envelope are defined, then the wind conditions, and then the definition of operational limits according to the DNV standard “DNV-OS-H101” is given.

### 2.3.1 Wave conditions

A sea state can be expressed with the spectrum of the wave amplitude versus the wave frequency. The wave environment in the North Sea is generally expressed with a JONSWAP-spectrum (Joint North Sea Wave Observation Project). The shape of this spectrum can be indicated with the significant wave height  $H_s$ , the mean value of the third-highest wave amplitudes, and the peak period  $T_p$ . The mean wind speed is the limiting factor during installation with a jack-up vessel. In order to aim this research at the same operational limits, the complementing significant wave height is taken for the limiting wind speed during the jack-up operation. The limiting wind speed is 10 m/s, the complementing significant wave height is approximately 2 m, based on GustoMSC experience. According to the empirical formulas presented in L. Li’s paper in 2015, a peak period of 4-10 s would result in a 95% non-exceedance level for a sight in the middle of the North Sea [19], these are the wave conditions that will be considered in this research. The wave direction in respect to the vessel is shown in Figure 2.3.1.

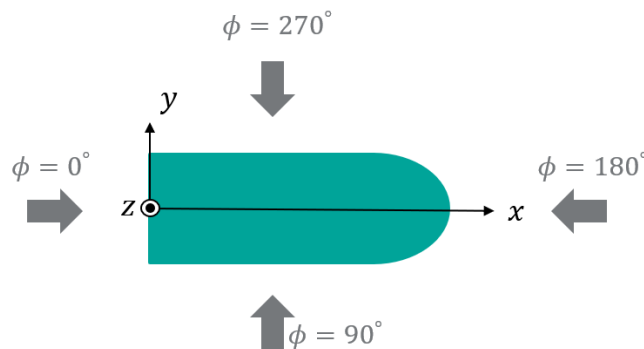


Figure 2.3.1: Wave direction in respect to the vessel

### 2.3.2 Wind conditions

The wind is a combination of a mean wind speed and a random gust:  $V(t) = V_{10} + V(t)$ . The amplitude of the varying part of the wind speed can be described with a Kaimall-spectrum. The shape of the Kaimall spectrum is dependent on the mean wind speed over the last 10 minutes. Since the limiting mean wind speed during a jack-up blade installation is 10 m/s, this research will not consider the mean wind speeds exceeding 10 m/s.

### 2.3.3 Weather window

Criteria for the weather restricted operations are given in the DNV standard “DNV-OS-H101 Marine Operations, General”[8]. To define an operational limit, the duration of the operation is important. The reference period  $T_R$  of the operation is defined as:

$$T_R = T_{POP} + T_C \quad (2.1)$$

where  $T_{POP}$  is the planned operation time, and  $T_C$  is the estimated maximum contingency time. The planned operation time  $T_{POP}$  should be based on a reasonable conservative assessment of similar operations. The estimated contingency time  $T_C$  is 50% of  $T_{POP}$  when there is extensive experience with the operation.

Every piece of equipment and part of the installation has its operational limit. The operational limiting criteria  $OP_{LIM}$  is the lowest limiting weather condition of the entire operation and the equipment.

To account for uncertainty in monitoring and forecasting of the environmental conditions, the forecasted operational criteria  $OP_{WF}$  should also be determined. The  $OP_{WF}$  is defined as  $OP_{WF} = \alpha OP_{LIM}$ , where  $\alpha$  is dependent on whether the operational limit is a limiting wind or wave condition and what the reference period of the operation is. In this case, the limiting weather condition will be wave dependent. The operation will last less than 12 hours. In the North Sea, with a significant wave height of  $H_s = 1$  m,  $\alpha = 0.65$ , and for  $H_s = 2$  m,  $\alpha = 0.76$ .

The  $T_R$ ,  $T_{POP}$ , and  $T_C$  are shown in Figure 2.3.2. During this time, several weather forecasts are done. If the weather exceeds the  $OP_{WF}$ , the operation will be stopped.

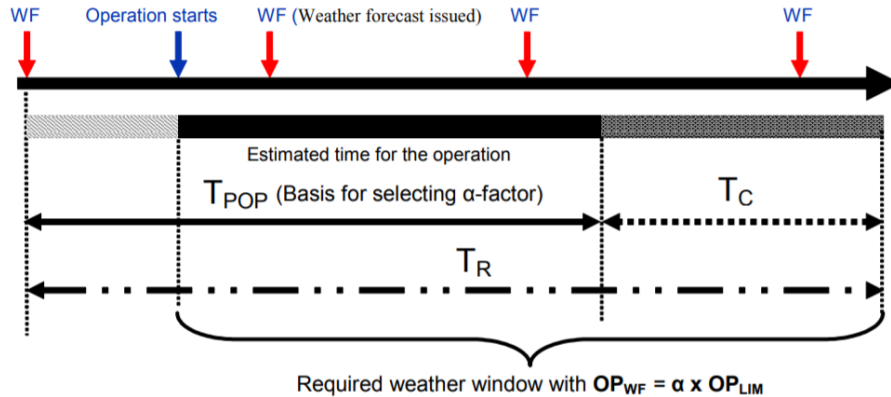


Figure 2.3.2: Illustration of the weather window (DNV-OS-H101 [8])

## 2.4 Concept selection

A concept lifting arrangement must be chosen for the single blade installation with a floating monohull crane vessel. Six concepts were proposed in the literature review on the determination of the optimal blade installation method with a floating vessel [18]. Each concept is based on using a limited amount of new technologies since the contractors have a large say in the used installation method of the wind turbines, and they are generally hesitant to use new technologies because it involves unknown risks. In all of the concepts, taglines were used to stabilize the blade. In the report, one concept was concluded to be the most feasible. The general steps of installation are illustrated in Figure 2.4.1 and 2.4.2 and can be described with the followed:

1. A blade gripper is attached to the crane hook. The taglines from the base of the crane are connected to the blade gripper.
2. The blade gripper is lifted from the deck and moved to the blade scaffolding, where the blade gripper picks up a blade from the scaffolding.
3. The crane rotates, and the blade is positioned parallel to the deck.
4. The blade is lifted upwards to hub height and horizontally aligned with the hub.
5. By monitoring the relative motion between the hub and the blade root, a moment is sought to move the blade closer to the hub and connect it to the hub. This final stage is called the mating phase.

The blade position is controlled with three compensation systems during the lifting procedure: two horizontal taglines to the crane boom, the blade gripper, and a crane line and taglines to the crane tip. Each compensation system works in one direction of the blade motions, x-, y-, or z-direction. By using three compensation systems in three directions, the motions of the blade are decoupled, which means that each direction can be controlled with a separate compensation system. A further explanation about the three control systems in the concept is discussed in Section 3.2.

## 2.5 Motion criteria during the critical phase

Two parts of the installation are most critical since much precision is needed to guarantee safety and structural integrity: when the blade is picked up from the scaffolding and the mating phase when the blade is connected to the hub. To determine the operational limits of the total system, the lowest environmental limits of the total system need to be sought. First, the critical phase with the lowest expected limits is selected, followed by a further elaboration of the motion criteria during this phase.

### 2.5.1 Critical phase selection

During the picking-up phase, the blade gripper must be positioned and connected to a blade in the scaffolding. The blade's center of gravity needs to be positioned precisely under the main hoist for stability during the installation. Lifting the blade out of the scaffolding needs to be done cautiously to avoid damage to the blade or the scaffolding.

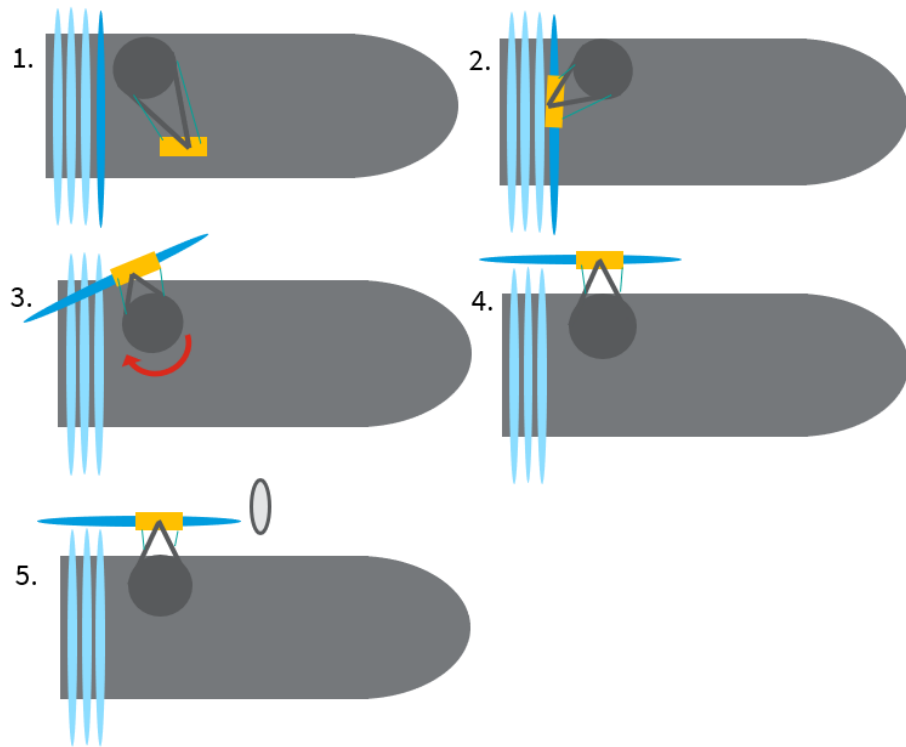


Figure 2.4.1: Top view of installation method

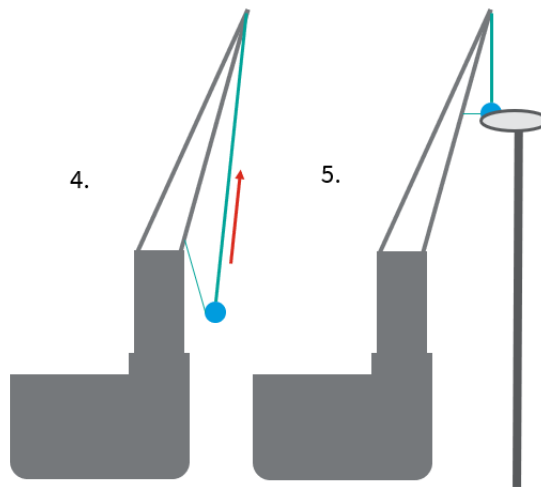


Figure 2.4.2: Front view of installation method

The mating phase is critical because there is a very small allowance for motions of the blade root while the connection between the blade root and the hub is made.

During the blade installation with a floating vessel, vessel motions will cause the crane to move. During the mating phase, the crane is operated at a large height where the crane tip motions can significantly impact the motions of the blade. During the picking-up phase, the crane tip motions can be compensated easier due to the large length of the crane line. Since the motion criteria for the mating phase is very small, this is the selected critical phase.

## 2.5.2 Motion criteria

The blade root has to be connected to the wind turbine hub in the mating phase. The pins of the blade need to fit precisely into the the wind turbine hub holes. Then, they need to be tightened by the crew inside the wind turbine hub. A motion limit is set on the allowed distance between the blade root and the hub, the distance is schematically shown in Figure 2.5.1. The maximum allowed distance  $d_{hb}$  is stated to be is 0.2 m in the thesis report of K. de Leeuw, made in cooperation with Van Oord BV [20]. The mating procedure lasts for a maximum period of 30 minutes [21].

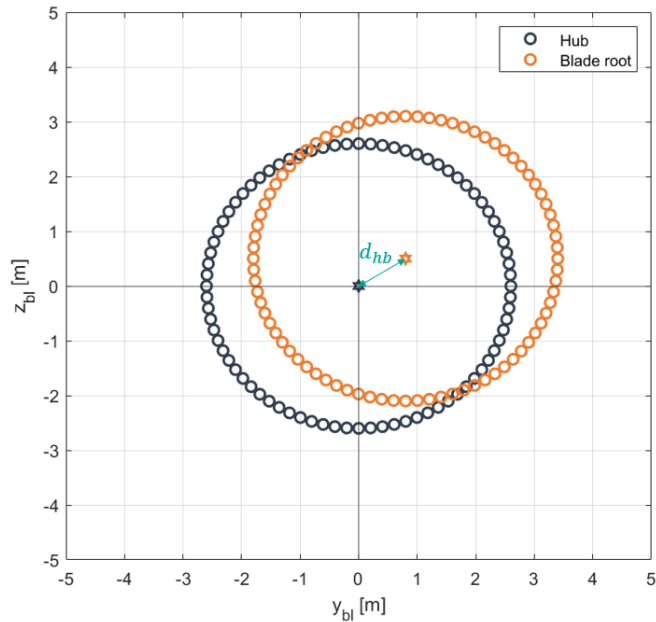


Figure 2.5.1: Distance between hub center and blade root center  $d_{hb}$



## 2.6 Conclusion

Multiple installation methods have been used in the industry for the installation of the rotor nacelle assembly. The single blade installation method is selected for further research to install wind turbine blades with a floating monohull crane vessel. Single blade installation is advantageous since, during blade maintenance, the entire hub or nacelle does not need to be decoupled to remove the blade from the turbine. Additionally, the single blade installation is the most used installation method, making it attractive for contractors who are hesitant to use new installation techniques.

The monohull crane vessel for this project is the GustoMSC EnsystXL. This vessel is a 280 meters long monohull crane vessel. The wind turbine blade used in this project is the blade of the IEA 15MW reference wind turbine.

Offshore installations are often weather restricted. The operational limit is the limiting wind or wave condition with which the operation can be realized safely. An environmental envelope is defined to find the operational limit of the single blade installation. The considered environmental envelope consists of wind and wave conditions that complement the operational limits of a single blade operation performed by a jack-up vessel.

A lifting concept with three dynamic controlled systems is proposed. The concept results from the literature review previous to this report. Each control system is designed to stabilize the position of the blade in a different direction. This concept is deemed most optimal for the stabilization of the blade position in space. Hence, this is the answer to the first subquestion. The three control systems will be discussed in more detail in Chapter 3.

The operational limits of the installation are based on one part of the installation; this is the critical phase. The selected critical phase of this installation is when the blade is aligned with the wind turbine hub, and the blade root is connected to the hub. This phase is deemed most critical due to the large operating height and the small motion criteria. This is the answer to the second subquestion.

The motion criteria are based on the distance between the blade root center and the center of the hub. The distance between the two must be less than 0.2 m. This is the answer to the third subquestion.

## 3 | Modeling of lifting arrangement

To find the operational limits, the critical phase of the lifting installation must be modeled. First, the degrees of freedom of the system are defined in Section 3.1. Then, the three control systems introduced in the previous chapter are discussed in 3.2, one of the systems is selected for the rest of the research. Assumptions need to be made for the control system model, these are described in Section 3.3. Then, all the equations of motion of the system are derived in Section 3.4. The chapter concludes with the discussion of the modeling strategy in Section 3.5.

### 3.1 Definition of degrees of freedom

Before making the model, the degrees of freedom (DOF) need to be defined. The entire installation consists of a vessel, a crane, the blade, and the crane- and taglines. All the degrees of freedom are shown in Figure 3.1.1 and 3.1.2. The degrees of freedom per body are:

Equipment	Modeled as	DOF	Generalized coordinate
Vessel	Rigid body	6	$x_s(t), y_s(t), z_s(t), \phi_s(t), \theta_s(t), \psi_s(t)$
Blade	Rigid body	6	$x_b(t), y_b(t), z_b(t), \phi_b(t), \theta_b(t), \psi_b(t)$
Crane	Rigid body (fixed on vessel)	0	
Crane line	Spring	2	$\theta_c(t), \gamma_c$

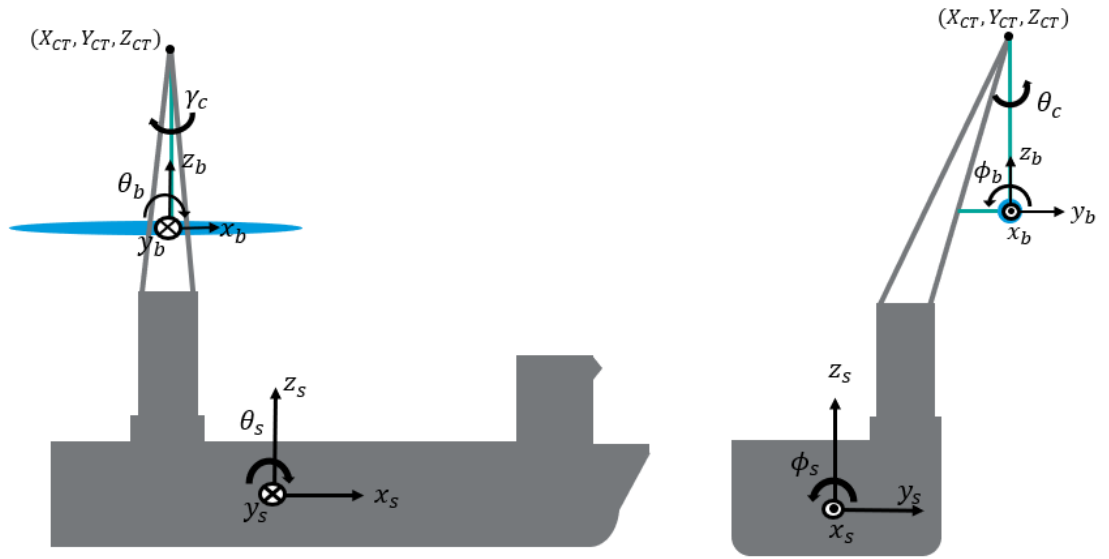


Figure 3.1.1: Side and front view of the installation vessel with blade [9]

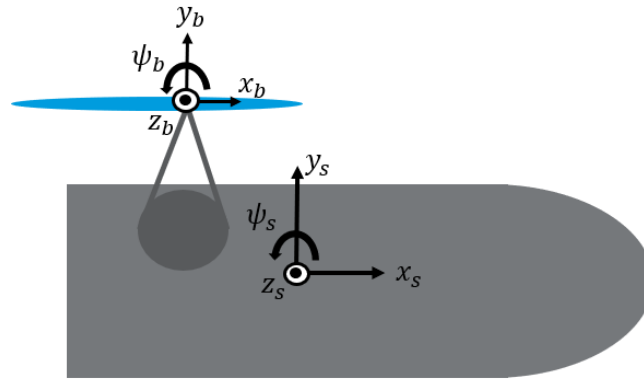


Figure 3.1.2: The top view of the installation vessel with blade

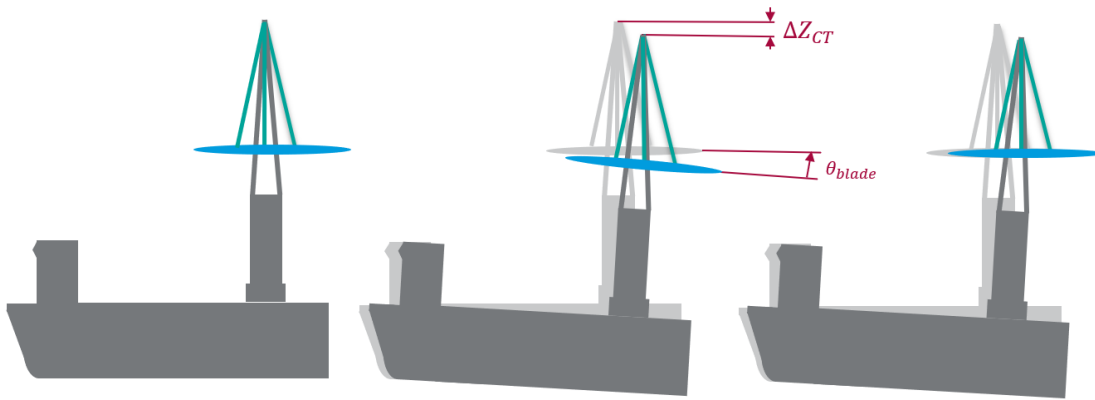
## 3.2 The compensation system concept

There are three separate compensation systems at work in the proposed lifting concept. When the motion of the blade is divided into six degrees of freedom, all degrees of freedom are stabilized using three different compensation systems: in  $z$ - and  $\theta$ -direction with lines to the crane tip,  $x$ - and  $\phi$ -direction with the blade gripper, and  $y$ - and  $\psi$ -direction with horizontal taglines to the crane boom. The first two systems are shown schematically in Figure 3.2.1 and the last system is shown in Figure 3.2.2.

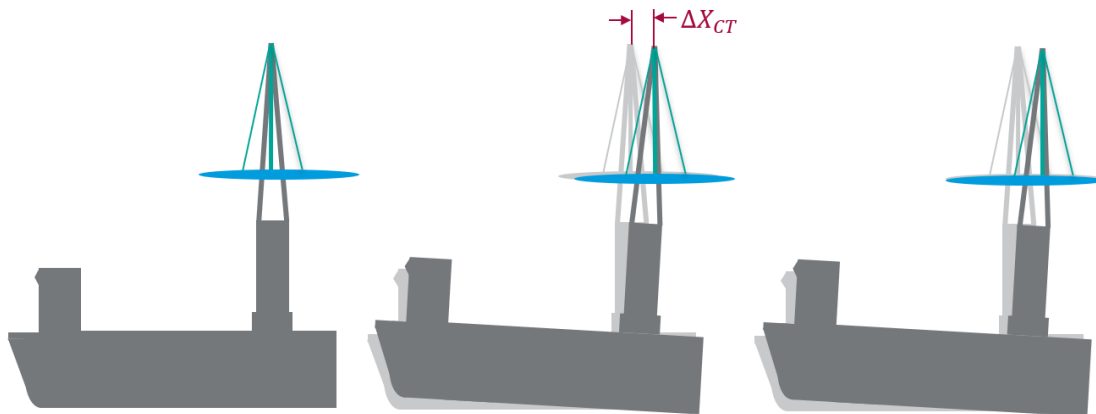
### 3.2.1 Overview and selection of compensation systems

The compensation in  $z$ - and  $\theta$ -direction are done with the main crane line and possibly more taglines to the top and bottom of the crane. However, compensating for the heave of the vessel is already widely executed in industry and thus is not the compensation system that will carry the focus of this research.

Compensation in the  $x$ -direction is challenging to execute with taglines to the vessel, which means the gripper itself or a line to an external point would need to compensate for the motions. The compensation for  $\phi_b$  is mainly solved by gravity, and the blade gripper is attached to the crane hook where it hinges. The gravity will keep the  $\phi_b$ -angle constant. Since the compensation in the  $x$ -direction is not done with taglines but rather with the blade gripper itself, this will not carry the focus of this research.



(a) Side view of vessel with compensation in  $z$ - and  $\theta$ -direction



(b) Side view of vessel with compensation in  $x$ -direction

Figure 3.2.1: Compensation systems in  $x$ -,  $z$ -, and  $\theta$ -direction

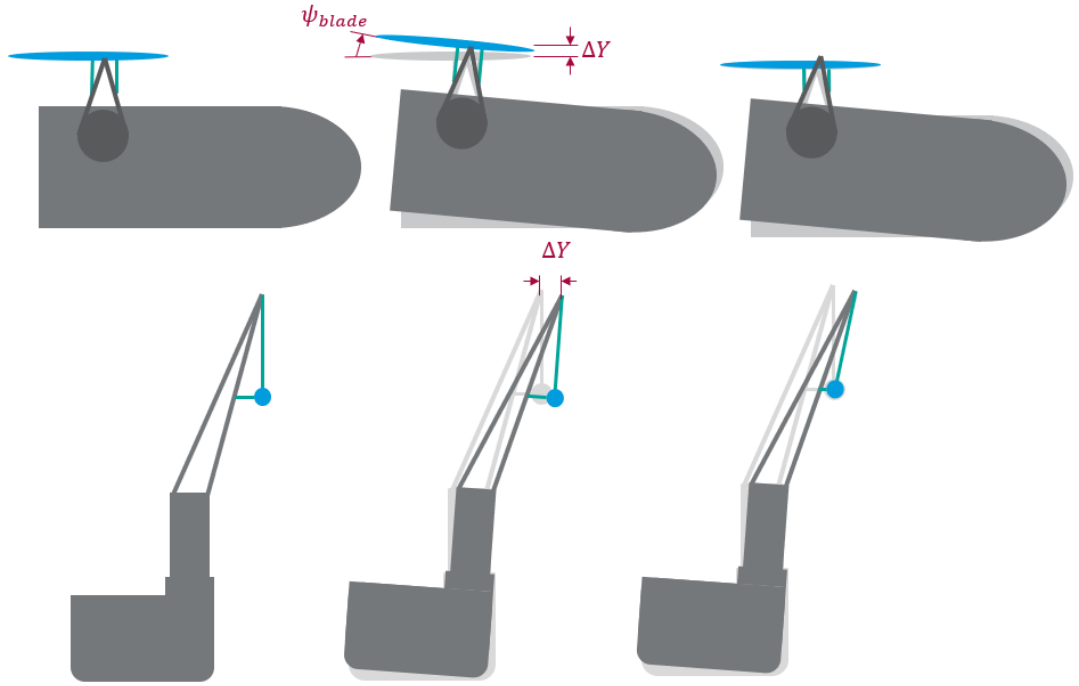


Figure 3.2.2: Top and front view of vessel with compensation in  $y$ - and  $\psi$ -direction

The  $y$ -motion of the blade is mainly caused by the roll, sway, and yaw motions of the vessel, as shown in Figure 3.2.2, and also to a smaller extent due to the wind loads. The global yaw angle of the blade is caused by the yaw motion of the vessel and the yaw angle of the blade around its  $z$ -axis. Since two horizontal taglines can control these motions to the crane boom, this will be the focus of this research.

The  $y$ -displacement of the blade is compensated with the total force applied on the blade by the two horizontal taglines, the  $\psi$  is compensated with the difference between the forces applied by the two taglines times the length of the blade gripper  $l_{bg}$ .

$$F_{tl} = F_1 + F_2 \quad (3.1)$$

$$M_{tl} = (F_1 - F_2)l_{bg} \quad (3.2)$$

With this approach, the  $y$ - and  $\psi$ -displacement can be decoupled. Hence, a separate feedback control system can be designed for both the  $y$ - and  $\psi$ -displacement.

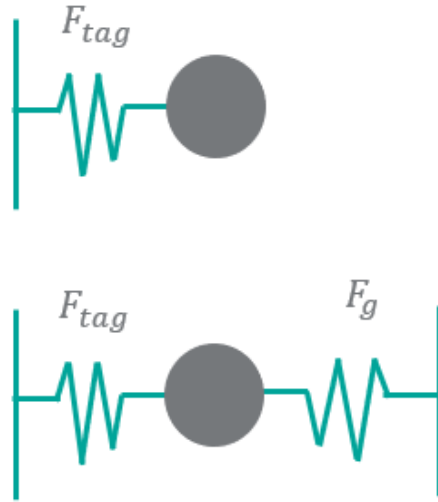


Figure 3.2.3: Situation 1 (top): Forces on the blade in y-direction without pretension. Situation 2 (bottom): Forces on the blade in y-direction with pretension.

### 3.2.2 Pretension

The blade can only be controlled by pulling taglines from one side. To provide a semi-controllable force in the opposite direction, a pretension is applied with the taglines. Then, the blade can be controlled with a pulling force towards the boom and with a gravitational force dependent on the crane line angle  $\theta_c$  and crane line length  $l_c$  in the opposite direction. The forces with and without pretension are shown in Figure 3.2.3, where  $F_{tag}$  is the y-force of both taglines combined, and  $F_g = m_b g l_c \sin \theta_c$ , where  $m_b$  is the blade mass,  $l_c$  the length of the crane line,  $g$  the gravitational constant, and  $\theta_c$  the angle of the crane line. There will always be tension in both directions when an adequate pretension is applied. When the blade displacement due to the pretension is smaller than the crane tip motions during an operation, there is no control in the positive y-direction of the blade.

The displacement in the y-direction can be controlled as long as the displacement due to the pretension is larger than the crane tip motions in the y-direction. However, the blade's speed and acceleration in positive y-direction depend on the crane line angle  $\theta_c$ , which is dependent on the pretension and the crane tip motion.

In this project, a pretension is applied on both the taglines to displace the blade 2 meters towards the crane boom.

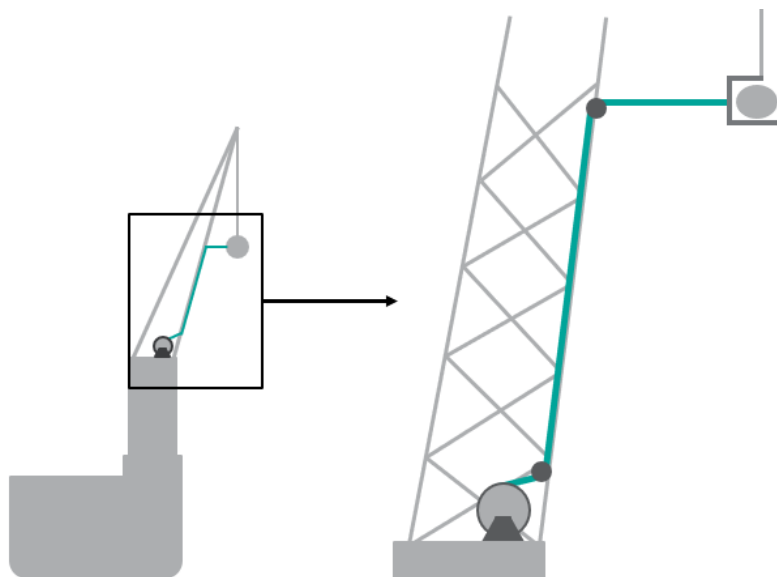


Figure 3.2.4: Schematic illustration of side-view of the winch system

### 3.2.3 Winches

The taglines of the compensation system are controlled by two winches on the bottom of the crane. Both winch mechanisms have two deflecting sheaves, as shown in Figure 3.2.4. To determine the needed capacity of the winches, the torque and torque speed need to be found.

The mean force provided by one winch used for the static displacement of the blade 2 m to the left is  $F_t = \frac{1}{2}m_b g \frac{l_{disp}}{l_c} = 118$  kN. Applying a 1.5 dynamic load factor, the maximum force applied during the installation is approximately 180kN. To compensate for efficiency losses and provide extra capacity, a winch is needed to pull a force of 200 kN. If a drum radius of 1 m is assumed, the torque of the winch should be at least 200 kNm.

The speed at which the winch should be able to pull is the relative speed between the blade and the crane boom at the location of the taglines. Since the blade is aimed to have little to no displacement, the speed of the boom is most important. In the literature review, a model was used where the most probable maximum motions of the crane tip were determined [18], the results of these calculations are used. To be conservative, the speed of the crane tip in the y-direction is considered: a maximum velocity of 0.76 m/s in three hours for a wave direction of  $150^\circ$ , an  $H_s$  of 2 m, and a  $T_p$  of 10 m. For a winch with a drum radius of 1 m, a torque speed of  $0.76/2\pi \cdot 60 = 7$  rpm is required.

In the overview of standardized offshore winches by Seatools, the power of 200kN and a speed of 7 rpm lays within the range of the winch capacity that they can provide [22]. Hence, in this project, the capacity of the winches is not assumed to be a limiting factor.

### 3.3 Assumptions

Assumptions need to be made to make a model. These are the most important ones for this project:

- Rigid body motions are used for the vessel and blade body motions.
- The weight of the blade and blade gripper is small compared to the crane's capacity. Hence, the deflection of the crane is neglected. The vessel body and the crane structure are assumed to be one rigid body.
- Tower dynamics are not considered. Realistically, the wind turbine hub has motion due to wave load excitation at the bottom of the tower. This is not taken into account; the wind turbine hub is assumed to have a constant position.
- The crane line is simplified to a massless bar attached from the crane tip to the blade.
- Wind loads on the vessel and blade gripper are neglected.
- The blade is assumed to be lifted directly above its center of gravity.
- Tagline forces are modeled as an external point load on the blades. The mass, stiffness, and damping of the lines are not considered.
- The tagline forces are modeled as a force in the y-direction. This means the angle of the taglines in the x-y-plane and z-y plane is not considered.
- The hydrodynamic damping on the vessel is assumed to be 5% of its critical damping in the roll direction. The aerodynamic damping on the blade is assumed to be 1% of its critical damping in the y-direction.
- No measurement noise or errors are considered in the measurements of the feedback control systems of the taglines.
- The weight of the blade, blade gripper, and crane hook is added together and is seen as one body.
- The blade motion in  $x_b$ -direction is assumed to be fully compensated by the compensation system in the blade gripper. Also, the pitch motion  $\theta_b$  of the blade is assumed to be compensated by the taglines to the crane tip.



### 3.4 Equations of motion

For the compensation system in the y-direction, the position of the blade root in the y-direction must be determined. The y-motion of the blade root can be expressed with the crane tip motion  $(y_{ct}, z_{ct})$ , the angle of the crane line  $(\theta_c)$ , the yaw angle of the ship  $(\psi_s)$  and the yaw angle of the blade  $(\psi_b)$ . With the tagline control system, only the  $\theta_c$  and  $\psi_b$  can be controlled, and the vessel motions are external disturbances on the blade. The equations of motion (EOM) of the  $\theta_c$  and  $\psi_b$  can be determined with the Lagrangian method. This is done in the following steps:

1. The degrees of freedom of the system are already defined in Section 3.1. However, for the y-motion of the blade, only the crane tip motions and the crane line angle are important, illustrated in Figure 3.4.1. Therefore, the crane tip motion in y-direction ( $y_{ct}$ ) and in z-direction ( $z_{ct}$ ) are used in the EOMs. The blade's global yaw angle depends on its yaw angle  $\psi_b$  and the yaw angle of the ship  $\psi_s$ . The time variable position of the blade needs to be determined using the available degrees of freedom.
2. The kinematic ( $T$ ) and potential energy ( $V$ ) of the system have to be determined.
3. Compute the Lagrangian ( $L$ ) of the system:  

$$L(q_i, \dot{q}_i, t) = T - V$$
4. Computing the equations of motion using the Euler-Lagrange's equation, shown in Equation 3.3, where the  $q_i$  is the generalized coordinates:  $\theta_c$  and  $\psi_b$ . The  $\dot{q}_i$  is the time derivative of the generalized coordinates:  $\dot{\theta}_c$  and  $\dot{\psi}_b$ .

$$F_{ext}(q_i) = \frac{d}{dt} \left( \frac{\partial L}{\partial \dot{q}_i} \right) - \frac{\partial L}{\partial q_i} \quad (3.3)$$

The motions of the blade can be expressed in terms of the vessel yaw motion  $\psi_s$  and angular crane line motions  $\theta_c$ , the position of the blade  $\mathbf{r}$  and the velocity  $\dot{\mathbf{r}}$ , and the yaw angle of the blade in the global axis system  $\psi_{blade}$ :

$$\begin{aligned} \mathbf{r} &= (y_{ct} + l_c \sin \theta_c) \mathbf{j} + (z_{ct} - l_c \cos \theta_c) \mathbf{k} \\ \dot{\mathbf{r}} &= (\dot{y}_{ct} + l_c \dot{\theta}_c \cos \theta_c) \mathbf{j} + (\dot{z}_{ct} + l_c \dot{\theta}_c \sin \theta_c) \mathbf{k} \\ \psi_{blade} &= \psi_b + \psi_s \\ \dot{\psi}_{blade} &= \dot{\psi}_b + \dot{\psi}_s \end{aligned}$$

The kinetic energy of the blade ( $T$ ) can be determined as given below.

$$T = \frac{1}{2} m_b \dot{\mathbf{r}}^2 + \frac{1}{2} I_{zz,b} \dot{\psi}_{blade}^2 \quad (3.4)$$

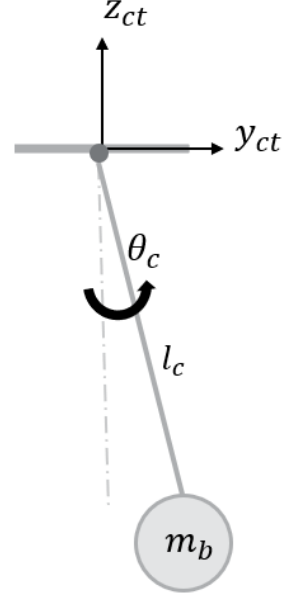


Figure 3.4.1: Pendulum model with moving base and a horizontally applied tagline force

The potential energy of the blade ( $U$ ) can be determined as stated below.

$$U = m_b g (z_{ct} + l_c (1 - \cos \theta_c)) \quad (3.5)$$

This makes the Lagrangian:

$$\begin{aligned} L = & \frac{1}{2} m_b l_c^2 \dot{\theta}_c^2 + m_b l_c \dot{\theta}_c (\dot{y}_{ct} \cos \theta_c + \dot{z}_{ct} \sin \theta_c) + \frac{1}{2} m_b (\dot{y}_{ct}^2 + \dot{z}_{ct}^2) \\ & + \frac{1}{2} I_{zz,b} (\dot{\psi}_b^2 + \dot{\psi}_s^2) + I_{zz,b} \dot{\psi}_s \dot{\psi}_b - m_b g (z_{ct} + l_c (1 - \cos \theta_c)) \end{aligned} \quad (3.6)$$

Solving Equation 3.3 with  $L$  for  $\theta_c$  and  $\psi_b$ , is done as followed:

$$\begin{aligned} 0 = & \frac{d}{dt} \left( \frac{\partial L}{\partial \dot{\theta}_c} \right) - \frac{\partial L}{\partial \theta_c} \\ = & \frac{d}{dt} \left( m_b l_c^2 \dot{\theta}_c + m_b l_c (\dot{y}_{ct} \cos \theta_c + \dot{z}_{ct} \sin \theta_c) \right) - \left( m_b l_c \dot{\theta}_c (-\dot{y}_{ct} \sin \theta_c + \dot{z}_{ct} \cos \theta_c) + m_b g l_c \sin \theta_c \right) \\ = & m_b l_c^2 \ddot{\theta}_c + m_b l_c (\ddot{y}_{ct} \cos \theta_c + \ddot{z}_{ct} \sin \theta_c) + m_b l_c g \sin \theta_c \end{aligned} \quad (3.7)$$

$$\begin{aligned} 0 = & \frac{d}{dt} \left( \frac{\partial L}{\partial \dot{\psi}_b} \right) - \frac{\partial L}{\partial \psi_b} \\ = & \frac{d}{dt} \left( I_{zz,b} (\dot{\psi}_b + \dot{\psi}_s) \right) \\ = & I_{zz,b} (\ddot{\psi}_b + \ddot{\psi}_s) \end{aligned} \quad (3.8)$$

While solving Equation 3.3, a linearization is applied:  $\cos \theta_c = 1$  and  $\sin \theta_c = \theta_c$ . This generates an error smaller than 1% as long as the angle  $\theta_c$  is smaller than  $8^\circ$ . Terms where two displacement, velocity, or acceleration motions are multiplied with each other, are neglected since the outcome will be much lower than the other terms.

The crane tip accelerations and yaw accelerations of the vessel translate into moments around the blade z-axis. Additionally, wind disturbances can also affect the blade position. Hence, the loads induced by the wind disturbances should also be included in the equations of motion. The wind loads that are considered are the wind load in the y-direction of the blade  $F_{y,wind}$ , and the moment the wind induces around the blade z-axis  $M_{z,wind}$ . The last external loads on the blade that are considered are the loads applied by the taglines: the force in y-direction  $F_{tl}$  (Equation 3.1), and the moment around the z-axis  $M_{tl}$  (Equation 3.2). The EOMs can be written in a matrix equation:

$$\begin{bmatrix} m_b l_c^2 & 0 \\ 0 & I_{zz,b} \end{bmatrix} \begin{bmatrix} \ddot{\theta}_c \\ \ddot{\psi}_b \end{bmatrix} + \begin{bmatrix} m_b g l_c & 0 \\ 0 & 0 \end{bmatrix} \begin{bmatrix} \theta_c \\ \psi_b \end{bmatrix} = \begin{bmatrix} -m_b l_c \ddot{y}_{ct} + (F_{y,wind} + F_{tl}) l_c \\ -I_{zz,b} \ddot{\psi}_s + M_{z,wind} + M_{tl} \end{bmatrix} \quad (3.9)$$

## 3.5 Modeling strategy

In this section, the difference between frequency and time domain modeling will be explained, the modeling strategy is given, and all the differences between the frequency domain model and the time domain model are listed.

### 3.5.1 Frequency and time domain modeling

Regular wave elevations are described as a constant sinusoidal formula. Within linear theory, an irregular wave elevation can be described as a summation of a large number of wave components:

$$\zeta(t, x) = \sum_{j=1}^N A_j \sin(\omega_j t - k_j x + \epsilon_j) \quad (3.10)$$

where  $A_j$ ,  $\omega_j$ ,  $k_j$ , and  $\epsilon_j$  are respectively the wave amplitude, circular frequency, wave number, and random phase angle between 0 and  $2\pi$ .

For deep water waves, the amplitude of the waves can be expressed in terms of a spectrum  $S_\zeta(\omega)$ , see Equation 3.11. The relation between the wave amplitude in the frequency domain and time domain is illustrated in Figure 3.5.1. The sea state is assumed to be stationary for a period of time between 0.5 and 10 hours. This is called a short-term description of the sea.

$$\frac{1}{2} A_j^2 = S_\zeta(\omega_j) \Delta\omega \quad (3.11)$$

where  $\Delta\omega$  is a constant frequency step in the spectrum.

The linear response of a vessel to wave elevation can be described with a frequency dependent transfer function, see Equation 3.12 where  $\eta_a(\omega)$  and  $\zeta_a(\omega)$  are respectively the frequency dependent vessel motion amplitude and wave elevation amplitude. In Equation 3.13, the derivation of the relation between the wave amplitude spectrum  $S_{\zeta\zeta}(\omega)$  and the response spectrum  $S_{\eta\eta}(\omega)$  is given with three steps.

$$RAO(\omega) = \frac{\eta_a(\omega)}{\zeta_a(\omega)} \quad (3.12)$$

$$\begin{aligned} S_{\eta\eta}(\omega) d\omega &= \frac{1}{2} \eta_a^2(\omega) \\ &= \left| \frac{\eta_a(\omega)}{\zeta_a(\omega)} \right|^2 \cdot \frac{1}{2} \zeta_a^2(\omega) \\ &= \left| \frac{\eta_a(\omega)}{\zeta_a(\omega)} \right|^2 \cdot S_{\zeta\zeta}(\omega) d\omega \\ S_{\eta\eta}(\omega) &= |RAO|^2 \cdot S_{\zeta\zeta}(\omega) \end{aligned} \quad (3.13)$$

This method can be used to describe any linear motion response on the vessel. As was mentioned in Section 2.3, the wind can also be partly described with a spectrum. The response to the dynamic part of the wind can thus also be described with a response spectrum. When one body is subjected

to both wind and wave loads, the response due to both is summed up to find the total response to the environmental conditions.

In a frequency domain calculation, non-linear effects cannot be considered. A non-linear effect is an effect or motion that cannot be described as a summation of sinusoidal terms, as described in Equation 3.10. A time domain simulation is required when a non-linear effect must be included in a calculation, and a linearization of the non-linear effect is not possible. For reproducing and verification of results, a time domain simulation uses randomness seeds to determine the random part of the simulation, like the  $\epsilon_j$  in Equation 3.10. With the Fourier transform theorem, a time series can be transformed to the frequency domain. The Fourier transfer function reads:

$$Y(j\omega) = \int_{-\infty}^{\infty} y(t)e^{-j\omega t} dt = \mathcal{F}\{y(t)\} \quad (3.14)$$

The benefit of using frequency domain calculations is that the simulation's running time is considerably lower than for time domain simulations. However, if more detail is required with non-linear effects, time domain simulations must be done.

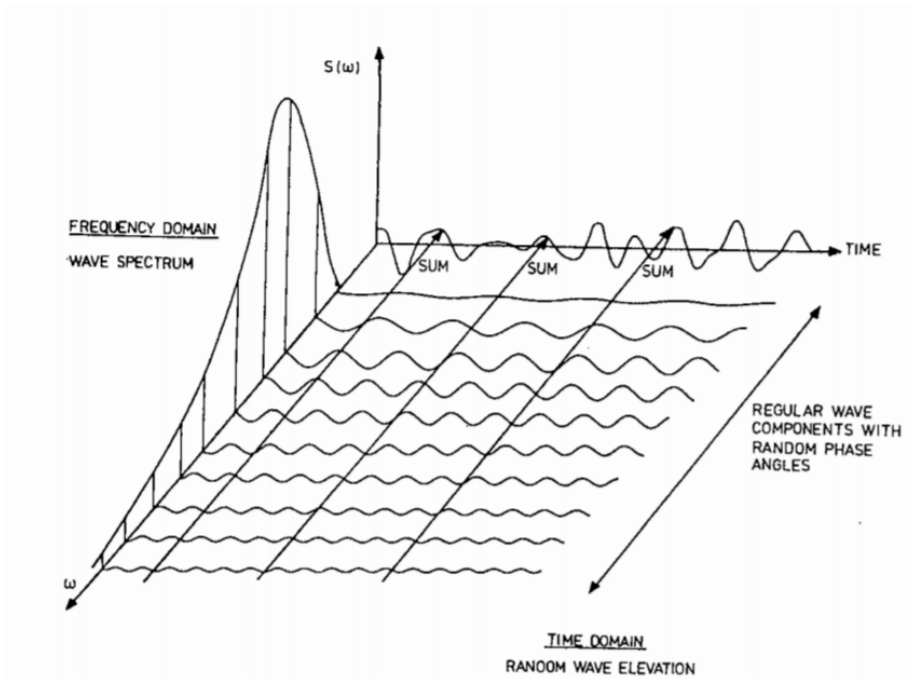


Figure 3.5.1: Illustration of the connection between time and frequency domain representation of a long crested short term sea state [10]

### 3.5.2 Strategy

Finding the operational limits of the blade installation is the goal of this research; to find these, the maximum blade root displacements must be determined for varying environmental conditions. The quickest way to find the maximum displacement of the blade is to use linear theory and model it in the frequency domain. The benefit of doing calculations in the frequency domain is that the motion and responses of a system can be determined in a short period of time because a frequency model does not take long to run. Statistical values can be deduced from the spectra, which can give a quick insight into the workings of the system. With those statistical values, the operational limits of the system can be determined. The downside of frequency domain calculations is that, since linear theory is used, all non-linear effects cannot be included in the calculations.

Looking at the tagline system, there are multiple non-linearities that are not included in the frequency domain calculations. One non-linearity is selected to be investigated in this research. In the frequency domain, the taglines can apply push and pull forces on the blade. However, the taglines are only able to apply pulling forces. The lifting concept includes a pretension on the taglines; this enables the blade to reach the reference position as long as the pretension causes a sufficient displacement towards the crane boom. However, the speed and acceleration of the blade in the opposite direction of the taglines are dependent on the blade mass and the angle of the crane line, which are both not directly controllable during the operation.

The controller parameters are dependent on the linearized system. This means the equation of motion needs to be determined for the blade y-position and blade angle  $\psi$  with one degree of freedom. Then, the operational limits can be determined within the frequency domain. To include the influence of the non-linearity of only having pulling taglines, time domain calculations must be done to confirm the operational limits and find new ones if the limits determined in the frequency domain are incorrect.

### 3.5.3 Differences between the time and frequency domain model

Two models will be made to determine the blade root displacements during the mating phase of a single blade installation: one in the frequency domain (FD) and one in the time domain (TD). These are the differences between the frequency and time domain model:

- In the TD model, the taglines are only able to apply pulling forces. In the FD model, the taglines both push and pull.
- Wave and wind loads are assumed to be independent in the FD model. In the TD model, this is not necessarily true.
- The relative wind speed at the blade is dependent on the speed of the wind and the speed of the blade itself. In the FD model, the speed of the blade is neglected. In the TD model, the speed of the blade is considered during the load calculation.
- In the TD model, springs are attached to the vessel body in  $x_s$ -,  $y_s$ - and  $\psi_s$ -direction to resemble a DP-system. The spring in  $x_s$ - and  $y_s$ -direction generate a natural frequency similar to the natural frequency in FD. The rotational spring in  $\psi_s$ -direction induces a natural frequency not considered in the FD model.
- In the calculation of the wind induced loads, the speed of the wind is squared. In the FD model, the wind speed is linearized, some of the wind loads are not considered. In the TD

model, linearization is not necessary, and thus the wind loads are determined over all the relative wind speed.

- The disturbance forces induced by the crane tip motions on the blade are linearized in the FD model. They are not linearized in the TD model.
- The PID-controller parameters are based on the linearized equation of motion of the y-displacement of the blade, which is also used in the FD model. The stability and performance is thus based on this linearized equation of motion. In the TD model, the same parameters are used but the motion of the blade y-displacement is not the same as the linearized EOM. The performance and the stability of the feedback systems might differ between the FD and TD models.
- The forces applied by the taglines on the blade work in the opposite direction on the crane boom. This is neglected in the FD mode; the tagline forces on the body are assumed not to influence the vessel motions. These forces on the vessel are included in the TD model.

### 3.6 Conclusion

In this chapter, the degrees of freedom of the system are defined, 14 degrees of freedom for the entire vessel, crane line, and blade model. Of the three compensation systems proposed in the previous chapter, one is selected: the compensation system for the blade motions in  $y$ - and  $\psi_{blade}$ -direction. With two taglines horizontally to the crane boom, the motions of the blade have to be compensated. A pretension is applied on the taglines to displace the blade towards the boom.

For a numerical model, assumptions need to be made. Some of the most important ones are:

1. Rigid body motions are used to determine the vessel and blade motions.
2. The tagline forces are modeled as external point loads on the blade, the tagline and winch mechanism are not considered.
3. The tagline forces only work in the  $y$ -direction.
4. In the feedback systems for the taglines, no measurement noise or errors are considered.

The equations of motion of the blade motions, dependent on the crane line angle  $\theta_c$  and the blade yaw angle  $\psi_b$ , are formulated. The EOMs are:

$$\begin{bmatrix} m_b l^2 & 0 \\ 0 & I_{zz,b} \end{bmatrix} \begin{bmatrix} \ddot{\theta}_c \\ \ddot{\psi}_b \end{bmatrix} + \begin{bmatrix} m_b g l_c & 0 \\ 0 & 0 \end{bmatrix} \begin{bmatrix} \theta_c \\ \psi_b \end{bmatrix} = \begin{bmatrix} -m_b l_c \ddot{y}_{ct} + (F_{y,wind} + F_{tl}) l_c \\ -I_{zz,b} \ddot{\psi}_s + M_{z,wind} + M_{tl} \end{bmatrix}$$

Then, the modeling strategy is discussed. This section answered subquestion 5, which was stated in the introduction. The most appropriate numerical modeling strategy is to first model the system in frequency domain and then model it in time domain after including the non-linearity of only pulling taglines. The operational limits should be determined with both models. The differences should be discussed to decide on how to define the operational limits.



## 4 | Tagline control

The taglines attached to the blade are controlled with two feedback systems. The force that should be applied by the taglines is dependent on both the  $y$ - and  $\psi$ -displacement of the blade. In Section 4.1, an introduction is given about the feedback controllers that are used for the taglines. The main components of the feedback loop are: the plant, the disturbance, and the controller. They are discussed respectively in Section 4.2, 4.3, and 4.4. The controller parameters are found with loop shaping. The loop shaping process and the results of the loop shaping process are given in Section 4.4.1.

### 4.1 Feedback control

The taglines are controlled with a feedback control system, schematically drawn in Figure 4.1.1. The terms in the figure are:

Abbreviation	Description
$r$	Reference position of the blade, the desired position of the blade
$y_m$	The measured position of the blade, what the sensors measure the position of the blade to be
$e$	error between the reference and measured position of the blade
Controller ( $C$ )	PID-controller, based on the input error a force is determined that should be applied to get the blade back to the reference position
$u$	Force determined by the controller to get the blade to the reference position
Disturbances ( $D$ )	Disturbance loads on the blade induced by the wind and the crane tip motions
Plant ( $P$ )	The blade responds to the forces applied by the controller and the disturbances, the new position of the blade is the output
$y$	New position of the blade

As was mentioned in Section 2.4, the  $y$ - and  $\psi$ -motion of the blade are decoupled. Hence, two separate single-input single-output (SISO) control systems are required. The controller for  $y$ -displacement determines the total force in  $y$ -direction needed to position the CoG of the blade in the correct position. The controller for  $\psi$ -displacement determines the moment that is needed to bring the angle back to its reference angle.



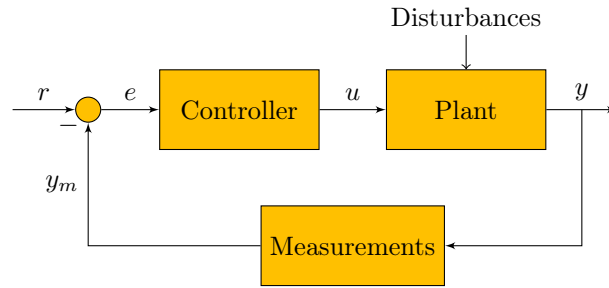


Figure 4.1.1: Basic feedback control system

### 4.1.1 Laplace-domain analysis

Within the feedback control system, the controller and plant transfer functions are described in the Laplace domain. The Laplace transformation of a periodic signal  $y(t)$  is similar to a Fourier transformation; however, the periodic signal  $y(t)$  is multiplied with  $e^{-\sigma t}$  before taking the Fourier-transform. The non-integratable signals can also be considered, this is called the Laplace-transform with variable  $s = \sigma + j\omega$ . The Laplace-transform function reads:

$$Y(s) = \mathcal{L}\{y(t)\} = \int_0^{\infty} y(t)e^{-st} dt \quad (4.1)$$

### 4.1.2 PID-controller

The controller is a PID-controller, schematically drawn in Figure 4.1.2. A PID-controller has three components that decrease the error between the reference position and the measured position. It corrects the proportional, derivative and integral error  $e$  with respectively a constant gain  $k_p$ ,  $k_d$ , and  $k_i$  as followed shown in Figure 4.1.2.

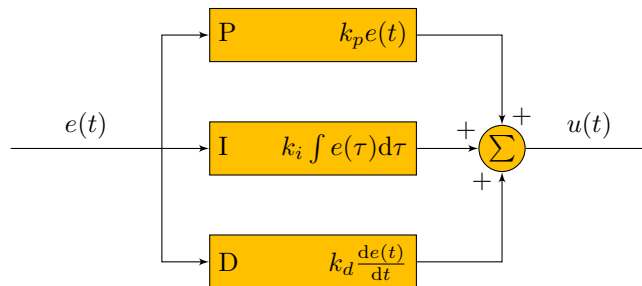


Figure 4.1.2: PID-controller

Proportional control corrects linearly for the error between the reference and measured position of the blade. Integral control corrects for the static mistake of the system, the error is integrated over time and thus the static mistake is compensated. The derivative control responds to the speed of the error, it damps the control signal. The performance and robustness of the system are dependent on the gain size. Hence, the appropriate gain sizes need to be sought to get the wished

result. Bode, Nyquist, and sensitivity plots can be used to find the appropriate gain sizes during the loop shaping process. However, firstly, the disturbances and the plant transfer functions need to be defined.

## 4.2 Plant transfer functions

The plant for the control system in  $y$ - and  $\psi$ -direction need to be defined. The plant is a linearized display of the blade motion. The plant of the feedback system is a transfer function between the  $y_b$  and an applied force, and the  $\psi_b$  and the applied moment. Since the feedback systems are single-input single-output systems, the plant must be based upon one degree of freedom.

### 4.2.1 Y-direction compensation

Two taglines are attached from the blade to the crane boom to manage the motion of the blade in the  $y$ -direction and compensate for the motions of the crane tip in the  $y$ -direction and wind loads on the blade. The summation of the two tagline forces is the force that will stabilize the blade. The system is simplified to a pendulum with a moving base, as shown in Figure 3.4.1. The force of the taglines works in the horizontal direction on the blade. As determined in Section 3.4, the equation of motion of the pendulum is:

$$m l_c^2 \ddot{\theta}_c(t) + m_b l_c g \theta_c(t) = M_{ext}(t) \quad (4.2)$$

where  $M_{ext}(t)$  is the external moment on the blade induced by the controller and the disturbances. In this case the external load consists of the total tagline force, the wind force in  $y$ -direction, and the force induced by the crane tip motion.

The plant  $P_y$  of the feedback system contains the transfer function between the  $y$ -position of the blade and the horizontally applied force on the mass. The EOM the  $y_b$ -position of the blade is introduced by substituting  $\theta_c = y_b/l_c$ :

$$m_b l_c \ddot{y}_b(t) + m_b g y_b(t) = F_{ext}(t) l_c \quad (4.3)$$

Taking the Laplace transform for of Equation 4.3 and writing it as the transfer function between the  $y_b$ -position of the blade and a force  $F$  applied on the blade, gives:

$$P_y(s) = \frac{y_b}{F} = \frac{1}{m_b s^2 + m_b \frac{g}{l_c}} \quad (4.4)$$

### 4.2.2 Yaw-compensation

The plant transfer function of the blade yaw motion is based on the equation of motion of the  $\psi_b$  is given in Section 3.4. For the feedback system the EOM for the  $\psi$ -motion is:

$$I_{zz}\ddot{\psi}_b(t) = M_{ext}(t) \quad (4.5)$$

The external moment  $M_{ext}(t)$  is the moment applied on the blade around its z-axis by the taglines, the wind, and the ship yaw moment. The plant equation, or transfer function of  $\psi$  to  $M$ , in Laplace-domain is:

$$P_\psi(s) = \frac{\psi_b(s)}{M(s)} = \frac{1}{I_{zz}s^2} \quad (4.6)$$

## 4.3 Disturbance loads

It is essential to first quantify the external forces induced on the blade to design the control system. Both the waves and the wind will (in)directly apply a load on the blade during the installation. A power spectrum is sought for the loads on the blade in y- and  $\psi_b$ -direction. In the EOM determined in Section 3.4, the crane tip motion and the vessel yaw motion were already included as an external force. The wind loads on the blade are dependent on the shape and angle of the blade and will also be quantified in this section.

### 4.3.1 Disturbance in blade y-direction

The wave loads on the ship induce ship motions, the linear response of the ship can be described with a response amplitude operator (RAO) shown in Appendix C. The software program called WAMIT is used to determine the frequency dependent wave induced forces  $F_j$  and hydrodynamic coefficients of the vessel,  $a_{kj}$ ,  $b_{kj}$ , and  $c_{kj}$ . The program uses a diffraction analysis where first order potential flow is used to solve the hydrodynamic coefficients in terms of frequency. With the calculated wave forces and the hydrodynamic coefficients, the RAO of the ship can be determined for different wave headings. The wave headings are shown in Figure 2.3.1.

The vessel motions translate into crane tip motions which need to be compensated by the control system to ensure a constant blade position. Hence, the crane tip motions should be investigated. Because the crane is assumed to be rigid, the crane tip motions can be determined using the vessel RAOs and rigid body dynamics:

$$\mathbf{s} = x_s\mathbf{i} + y_s\mathbf{j} + z_s\mathbf{k} + \boldsymbol{\omega} \times \mathbf{r}$$

with

$$\begin{aligned} \boldsymbol{\omega} &= \phi_s\mathbf{i} + \theta_s\mathbf{j} + \psi_s\mathbf{k} \\ \mathbf{r} &= X_{ct}\mathbf{i} + Y_{ct}\mathbf{j} + Z_{ct}\mathbf{k} \end{aligned}$$

where  $\mathbf{i}$ ,  $\mathbf{j}$ , and  $\mathbf{k}$  are unit vectors along the x-, y-, and z-axis. This results in the following expression:

$$\mathbf{s} = (x_s + Z_{ct}\theta_s - Y_{ct}\psi_s)\mathbf{i} + (y_s - Z_{ct}\phi_s + X_{ct}\psi_s)\mathbf{j} + (z_s + Y_{ct}\phi_s - X_{ct}\theta)\mathbf{k} \quad (4.7)$$

The disturbance load on the blade in y-direction caused by the crane tip motions in y-direction is given in Equation 3.9 as:  $-m_b l_c \ddot{y}_{ct}$ . To translate wave spectra to a spectrum for  $y_{ct}$  acceleration, the  $RAO_{\zeta \ddot{y}_{ct}}$  is needed to find the disturbance load on the system. The  $RAO_{\zeta \ddot{y}_{ct}}$  is calculated using the previously explained rigid body dynamics.

The wave spectra  $S_{\zeta \zeta}$  discussed in Section 2.3 that form the environmental envelope can be multiplied with the  $RAO_{\zeta \ddot{y}_{ct}}$  to find the crane tip acceleration spectrum (Equation 4.8), and then the disturbance spectrum (Equation 4.9). The disturbance power spectrum is given in Figure 4.3.1 for a wave direction of  $165^\circ$ , a significant wave height of  $H_s = 2$  m, and a peak period  $T_p = 4-10$  s.

$$S_{\ddot{y}_{ct} \ddot{y}_{ct}}(\omega) = |RAO_{\zeta \ddot{y}_{ct}}(\omega)|^2 S_{\zeta \zeta}(\omega) \quad (4.8)$$

$$S_{F_w F_w}(\omega) = m_b^2 S_{\ddot{y}_{ct} \ddot{y}_{ct}}(\omega) \quad (4.9)$$

The wind loads also apply a force on the blade. The force on one segment of the blade can be determined with the drag and lift of the blade. The drag and lift force are dependent on the angle of attack of the wind on the blade. The equation for the lift and drag force are:

$$F_{L,i} = \frac{1}{2} \rho_a A_i C_l(AOA_i, (t/c)_i) V^2 \quad (4.10)$$

$$F_{D,i} = \frac{1}{2} \rho_a A_i C_d(AOA_i, (t/c)_i) V^2 \quad (4.11)$$

where  $\rho_a$  is the air density in  $\text{kg/m}^3$ ,  $A_i$  is the area of the segment calculated with  $A_i = \frac{\text{Chord}_i + \text{Chord}_{i+1}}{2} (y_{end,i} - y_{begin,i})$ ,  $C_l$  and  $C_d$  are the lift and drag coefficient dependent on the angle of attack which is determined with the wind angle, twist of the blade, and the pitch angle of the blade:  $AOA_i = \theta_w - \text{twist}_i + \theta_p$ ,  $V$  is the wind speed in m/s. The lift and drag force can be projected on the y-axis to determine the force in y-direction per segment. Then, the force on each segment added up:

$$F_{y,i} = F_{L,i} \sin(\theta_w) - F_{D,i} \cos(\theta_w) \quad (4.12)$$

$$F_{y,wind} = \sum_{i=0}^{\text{blade end}} F_{y,i}$$

If the angle of the twist and pitch of the blade do not change over time, the force in the y-direction can also be described as follows:

$$F_{y,wind} = \frac{1}{2} \rho_a V^2(t) \xi_f \quad (4.13)$$

$$\xi_f = \sum_{i=0}^{\text{blade end}} A_i (C_{L,i} \sin(AOA(\text{twist}_i)) - C_{D,i} \cos(AOA(\text{twist}_i)))$$

The wind speed is a random process around a mean wind speed:  $V(t) = V_0 + v(t)$ . Assuming the time variant wind speed is small, the  $v^2(t)$  term in Equation 4.13 can be linearized to:  $V^2(t) = V_0^2 + 2V_0 v(t)$ . This indicates that the mean force due to a constant wind can be determined with Equation 4.14. The mean blade force in y-direction for a mean wind speed of 2-10 m/s and a wind inflow angle of  $10^\circ$  is calculated using the blade parameters given in Appendix A.3 and

presented in Table 4.3.1. The variable part of the wind speed can be determined using a Kaimal-spectrum dependent on the mean wind speed  $V_0$  as shown in Equation 4.15, with the turbulence  $I$ , a turbulence length scale  $l$ , and frequency  $f$ .

$$F_{y,0} = \frac{1}{2}\rho_a\xi_f V_0^2 \quad (4.14)$$

$$S_{vv}(\omega) = \frac{4I^2 V_0 l}{(1 + 6\frac{\omega l}{2\pi V_0})^{5/3}} \quad (4.15)$$

The relation between the varying wind speed and the moment on the blade can be determined with:

$$H_{F_{y,v}} = \frac{F_y}{v} = \rho_a\xi_f V_0 \quad (4.16)$$

The spectrum for varying y-force on the blade is calculated with Equation 4.17. Using the blade parameters and  $I=0.14$  and  $l=340.2$  m, the  $S_{F_{y,wind}F_{y,wind}}$  for a mean wind speed of 2 to 10 m/s is shown in Figure 4.3.1.

$$S_{F_{y,wind}F_{y,wind}}(\omega) = |H_{F_{y,v}}|^2 S_{vv}(\omega) = |\rho_a\xi_f V_0|^2 S_{vv}(\omega) \quad (4.17)$$

Table 4.3.1: Mean force in blade y-direction due to a mean wind speed of 2-10 m/s

$V_0$ [m/s]	2	3	4	5	6	7	8	9	10
$F_{y0}$ [N]	164.5	370.1	658.0	1028.1	1480.5	2015.1	2632.0	3331.1	4112.5

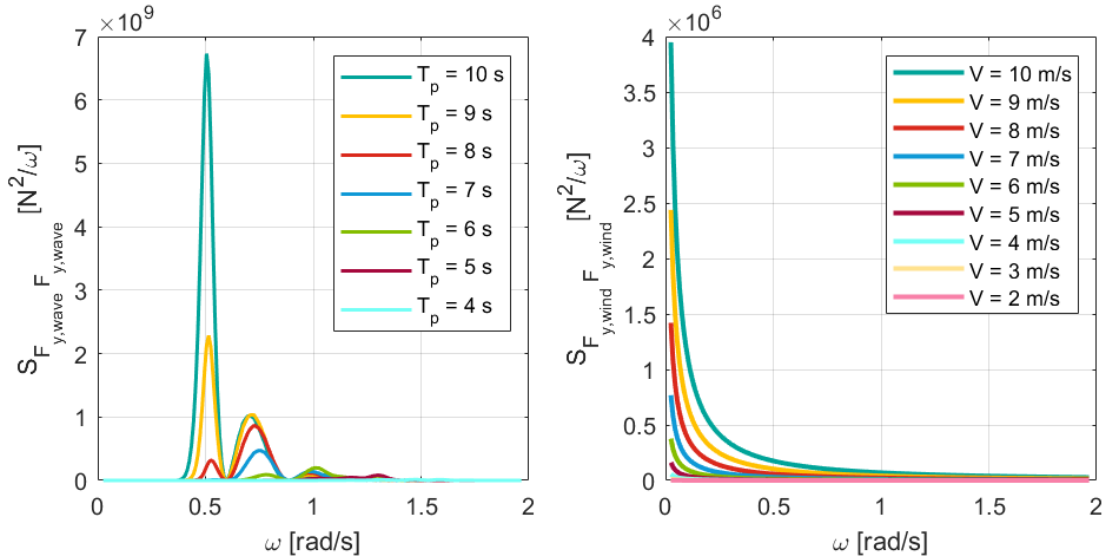


Figure 4.3.1: Force spectrum of wave and wind induced forces on the blade

### 4.3.2 Disturbance on the $\psi_b$ -motion of the blade

The moment induced on the blade due to the ship yaw motion, from Equation 3.9, is:  $-I_{zz,b}\ddot{\psi}_s$ . Hence, to determine the wave induced loads on the blade in  $\psi_b$ -direction, the spectrum  $S_{\ddot{\psi}_s\ddot{\psi}_s}$  is needed. Since the RAOs of the vessel motions are known from the WAMIT data, the RAO $_{\psi_s\zeta}$  is known. With this, the response spectrum of the vessel yaw motion can be determined using Equation 4.18. Then, the  $S_{\ddot{\psi}_s\ddot{\psi}_s}$  can be determined using Equation 4.19. Using the equation of motion, the moment spectrum can be determined with Equation 4.20. The moment spectrum induced by the vessel motions is shown in Figure 4.3.2

$$S_{\psi_s\psi_s}(\omega) = |RAO_{\zeta\psi_s}(\omega)|^2 S_{\zeta\zeta}(\omega) \quad (4.18)$$

$$S_{\ddot{\psi}_s\ddot{\psi}_s}(\omega) = \omega^4 S_{\psi_s\psi_s}(\omega) \quad (4.19)$$

$$S_{M_z, wave}(\omega) = I_{zz,b}^2 S_{\ddot{\psi}_s\ddot{\psi}_s}(\omega) \quad (4.20)$$

The  $\psi$ -angle of the blade is also influenced by wind loads. When the force in y-direction due to the wind per segment (Equation 4.12) is multiplied with the distant from the segment to the CoG of the blade, the wind induced moment on the blade can be determined.

$$M_{z, wind} = \sum_{i=0}^{blade\ end} F_{y,i} y_i \quad (4.21)$$

If the angle of the twist and pitch of the blade do not change over time, the moment around the z-axis can be described as followed:

$$M_z = \frac{1}{2} \rho_a V^2(t) \xi_m \quad (4.22)$$

$$\xi_m = \sum_{i=0}^{blade\ end} A_i y_i (C_{L,i} \sin(AOA(twist_i)) - C_{D,i} \cos(AOA(twist_i)))$$

As discussed in the previous section, the wind speed is partly a mean force and partly time dependent  $V(t) = V_0 + v(t)$ . Assuming the time variant wind speed is small, the  $V^2(t)$  term in Equation 4.22 can be linearized to:  $V^2(t) = V_0^2 + 2V_0v(t)$ . This indicates that the mean moment due to a constant wind can be determined with Equation 4.23. The mean blade moment around the z-axis for a mean wind speed of 2-10 m/s and a wind inflow angle of  $10^\circ$  is calculated using the blade parameters given in Appendix A.3 and presented in Table 4.3.2. The variable part of the wind speed can be calculated with Equation 4.15.

$$M_{z,0} = \frac{1}{2} \rho_a \xi_m V_0^2 \quad (4.23)$$

The relation between the varying wind speed and the moment on the blade can be determined with:

$$H_{M_z v} = \frac{M_z}{v} = \rho_a \xi_m V_0 \quad (4.24)$$

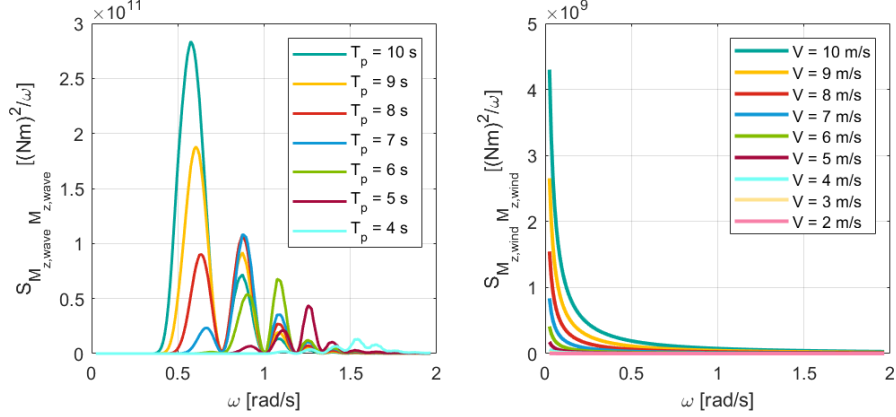


Figure 4.3.2: Moment spectrum around the blade z-axis due to wind and wave loading

The spectrum for varying z-moment on the blade is calculated with Equation 4.25. Using the blade parameters and  $I=0.14$  and  $l=340.2$  m, the  $S_{M_{z,wind}M_{z,wind}}$  for a mean wind speed of 2 to 10 m/s is shown in Figure 4.3.2.

$$S_{M_{z,wind}M_{z,wind}}(\omega) = |H_{M_z v}|^2 S_{vv}(\omega) = |\rho_a \xi_m V_0|^2 S_{vv}(\omega) \quad (4.25)$$

Table 4.3.2: Mean moment around blade z-axis due to a mean wind speed of 2-10 m/s

$V_0$ [m/s]	2	3	4	5	6	7	8	9	10
$M_{z0}$ [kNm]	107.2	241.3	428.9	670.2	965.1	1313.5	1715.6	2171.4	2680.7

## 4.4 Controller parameters

The gain sizes of the PID-controller need to be found. They can be defined during a loop shaping process. In this section, the main objectives of the loop shaping process are described, then the resulting gain sizes are given.

### 4.4.1 Loop shaping process

The appropriate gain sizes of the PID-controller are found by shaping the loop transfer function  $L(s)$ ; this is the multiplication of the control- and the plant transfer function:

$$L(s) = P(s) \cdot C(s) = P(s) \cdot \frac{1}{\frac{1}{s}(k_p s + k_i + k_d s^2)} \quad (4.26)$$

where  $P(s)$  is the  $P_y(s)$  and  $P_\psi(s)$  determined in Section 4.2.

There are two loop shaping methods to consider: tracking or disturbance rejection. In a tracking problem, the controller is focused on tracking a given input. In our system, the reference position of the blade is one position. Hence, the focus of the controller is not necessarily to follow a reference point. Hence, this is not an adequate starting point for the loop shaping.

Disturbance rejection focuses on designing a control system for a random disturbance in a known frequency range. It uses a reference position for the blade; in the mating procedure, this is the location just in front of the wind turbine hub. All external forces due to crane tip motions and wind are categorized as a disturbance. The goal of the control system is to let the disturbances affect the plant as least as possible.

Several aspects must be considered during the loop shaping process. Here is a summation of the aspects:

1. To ensure the system's stability, the closed-loop poles must have a negative real part. The closed-loop transfer function gives the relation between the input and output of the closed-loop:

$$G_{yu}(s) = \frac{L(s)}{1 + L(s)} \quad (4.27)$$

2. In the Nyquist plot, the curve must not cross or encircle the critical point. The critical point is the point where the angle of the loop transfer function  $\angle L(i\omega)$  is equal to  $-180^\circ$ , and the magnitude of  $L(i\omega) = -1$ . The signal is  $180^\circ$  out of phase at this critical point and has a magnitude larger than 1; this means the system would be unstable.
3. The bandwidth of the closed-loop transfer function. The closed-loop transfer function resembles how the controller can keep the blade at the reference position. At the frequency where the loop transfer function crosses 1 and keeps decreasing, the controller influence on the blade decreases exponentially. Since the motion of the crane tip is the disturbance that will be considered, the largest frequency that will be taken into account is associated with the RAO of the crane tip motion in the y-direction.
4. Increasing the bandwidth lowers the gain margin. The gain margin  $g_m$  and phase margin  $\phi_m$  should have an appropriate size to provide robustness in the control system. There will be differences between the simplified model of the plant and the actual installation vessel. By having a sufficient gain and phase margin, the chance of sustaining stability in the real system increases. A reasonable phase margin is between  $30^\circ$ - $60^\circ$ , a reasonable gain margin between 2-5 [23].
5. The load sensitivity function resembles how much the blade position reacts to a disturbance load. It is desirable to keep this effect as low as possible to induce minimum displacement for a disturbance load. The load sensitivity function is as follows:

$$G_{dy}(s) = \frac{P(s)}{1 + P(s) \cdot C(s)} \quad (4.28)$$

A disturbance load is the load induced by motion of the crane tip or the wind loads.

Taking all of the criteria into account, the constants  $K_p$ ,  $K_i$ ,  $K_d$  and  $\omega_{lp}$  of Equation 4.29, and the system properties are concluded and shown in Table 4.4.1 and Table 4.4.2.



The gain margin of both systems is infinite; this suggests that the bandwidth could be increased infinitely without the system becoming unstable. However, there are many high frequencies at work in practice, and thus, a higher bandwidth is not feasible. The  $\omega_{lp}$  is the lowpass frequency; the sensitivity to high frequency signals is filtered out by adding this to the equation. In the following subsection, this will be elaborated further.

The phase margin for the yaw system is larger than what was deemed appropriate. However, the phase margin could not be decreased because the plant transfer function  $P_\psi$  is just a mass in space without a spring or damping term in the equation of motion.

$$u(s) = \frac{1}{s} \left( K_p s + K_i + K_d s^2 \frac{\omega_{lp}}{s + \omega_{lp}} \right) \quad (4.29)$$

Table 4.4.1: PID-controller parameters for  $y$ -compensation

$K_p$	$K_i$	$K_d$	$\omega_{lp}$ [rad/s]	$g_m$	$\phi_m$	poles		
2.28e+06	3.05e+05	4.25e+06	2	Inf.	38°	0.00	+	0.00i
						-0.24	+	0.00i
						-0.70	+	1.18i
						-0.70	-	1.18i
						0.00	+	0.63i
						0.00	-	0.63i

Table 4.4.2: PID-controller parameters for  $\psi$ -compensation

$K_p$	$K_i$	$K_d$	$\omega_{lp}$ [rad/s]	$g_m$	$\phi_m$	poles		
2.36e+09	2.44e+09	5.56e+08	2	Inf.	75°	0.00	+	0.00i
						-263.16	+	0.00i
						-235.69	+	0.00i
						-22.52	+	0.00i
						-3.34	+	0.00i
						-1.61	+	0.00i

#### 4.4.2 Lowpass filter

Many high frequencies are at work in offshore structures or vessels, caused by the onboard generators and machines, which is why sensors typically have high frequency noise in their signals. The derivative control goes to infinity for an infinite frequency, thus a large response can be induced by these high frequencies. A lowpass filter decreases the derivative control for high frequencies to prevent large responses to non-intended excitations. Even though these frequencies are not at work in the frequency and time domain model, a lowpass filter is added. The lowpass filter is set at  $\omega_{lp} = 2$  rad/s since the wind and wave excitation are both below 2 rad/s and no response is needed for higher frequencies.

## 4.5 Conclusion

In this chapter, the components of the feedback system in Laplace-domain are defined. The plant transfer function is formulated, the disturbance loads by crane tip displacements and wind loads are defined in frequency domain. Based on the plant transfer function and the disturbances, a loop shaping process is followed with which the gain sizes of the PID-controller are defined.



# 5 | Frequency domain model

The operational limits according to frequency domain calculations can be found now that the terms for the plant, disturbance, and controller of the feedback systems are defined. First, a model description will be given in Section 5.1. Then, the results are given and discussed in Section 5.2.

## 5.1 Model description

With the transfer function of the plant and controller in place, the performance of the feedback system can be mapped out in the frequency domain. First, the system's performance in y-direction will be considered, followed by a look into the  $\psi$ -compensation system.

The following assumptions are made to perform the frequency domain analysis:

- All results are based on the steady-state performance of the system; transient effects are not considered.
- The taglines can apply both push and pull forces.
- The controllers are assumed to be stable.
- The relative wind speed caused by the swinging of the blade is neglected.
- Any influence that the blade motions or the tagline forces on the crane boom have on the vessel motions are neglected.

### 5.1.1 Y-compensation power spectra and maxima

The disturbance power spectrum on the blade induced by several wind and wave conditions is given in Figure 4.3.1. The disturbance sensitivity function is the transfer function between disturbance and blade y-displacement. Hence, the blade y-displacement spectrum can be determined with 5.1.

$$S_{y_b y_b}(\omega) = \left| \frac{P_y(\omega)}{1 + C_y(\omega)P_y(\omega)} \right|^2 S_{F_w F_w}(\omega) \quad (5.1)$$

To distinguish the effect of using feedback controlled taglines, the blade displacement is also determined for a case where no control is used on the taglines. Then, the motion spectrum of the blade is determined without using the feedback loop and the controller:

$$S_{y_b y_b}(\omega) = |P_y(\omega)|^2 S_{F_w F_w}(\omega) \quad (5.2)$$

The most probable maximum displacement of the blade in the y-direction can be determined using its power spectrum with Equation 5.3 for a reference period of 30-minutes. The  $N$  is the number of cycles in the reference period, determined with  $N = 1800/T_p$ . This calculation of the most probable maximum value assumes that the maximum values are Rayleigh distributed, narrow-banded and that the maximum values are independent of each other.

$$\begin{aligned}
y_{b,mpm} &\approx \sigma_{y_b} \sqrt{2 \ln N} \\
\sigma_{y_b} &= \sqrt{m_0} \\
m_0 &= \int_0^\infty \omega^0 S_{y_b y_b}(\omega) d\omega
\end{aligned} \tag{5.3}$$

### 5.1.2 $\psi$ -compensation power spectra and maxima

The yaw of the blade induces a displacement of the blade root; the blade root displacement should be contained to keep it within the criteria boundaries. To inspect the frequency sensitivity, the power spectrum of the blade root displacement is determined with the power spectrum of the wind induced moment around the blade z-axis, the disturbance sensitivity function between the wind moment and the  $\psi$ , and the distance between the blade CoG and the blade root  $l_{br}$ :

$$S_{\psi\psi}(\omega) = \left| \frac{P_\psi(\omega)}{1 + C_\psi(\omega)P_\psi(\omega)} \right|^2 S_{M_z M_z}(\omega) \tag{5.4}$$

$$S_{y_{br} y_{br}}(\omega) = |l_{br}|^2 S_{\psi\psi}(\omega) \tag{5.5}$$

To compare the feedback controlled system results, a response spectrum is determined for the non-controlled yaw motion. Since the EOM for  $\psi_b$  does not include any spring term, the blade's maximum y-displacement will become very large because the blade does not have any force to counter a spinning motion. To prevent the blade from spinning, a spring term of  $k_{\psi,b} = 4 \cdot 10^6$  Nm/rad is added, for which the natural frequency of  $\psi_b$  becomes approximately 15 s. Then, the equation for the plant  $P_\psi$  becomes:

$$P_\psi(\omega) = \frac{1}{I_{zz}s^2 + k_{\psi,b}} \tag{5.6}$$

The blade root displacement spectrum without control is:

$$S_{y_{br} y_{br}}(\omega) = |P_\psi(\omega)l_{br}|^2 S_{M_z M_z}(\omega) \tag{5.7}$$

For the situation with and without control, the  $y_{br,mpm}$  is determined as:

$$\begin{aligned}
y_{br,mpm} &\approx \sigma_{y_{br}} \sqrt{2 \ln N} \\
\sigma_{y_{br}} &= \sqrt{m_0} \\
m_0 &= \int_0^\infty \omega^0 S_{y_{br} y_{br}}(\omega) d\omega
\end{aligned} \tag{5.8}$$

### 5.1.3 Blade root displacements for combined wind and wave loads

When both the wind and wave spectra are combined, a double peaked load spectrum is applied to the blade. The  $y_{mpm}$  can therefore not be determined with a number of cycles  $N$ . When both wind and wave loads are applied to the system, the most probable maximum can be approximated as follows:

$$y_{tot,mpm} = \sqrt{y_{b,mpm}^2 + y_{br,mpm}^2} \quad (5.9)$$

where  $y_{b,mpm}$  is the blade displacement in y-direction due to the crane tip displacement in the y-direction, and  $y_{br,mpm}$  is the blade root displacement due to the wind induced moment on the blade.

### 5.1.4 The operational limits

The operational limits for a wave direction of  $165^\circ$  and  $150^\circ$  can be determined using the linear theory. Since there is no y-motion when the wave direction is  $180^\circ$ , the operational limit for this wave direction is infinity.

To find the significant wave height with which the most probable maximum y-displacement reaches the motion limit of 0.2 m, the following equation can be used:

$$H_{s,lim} = \frac{0.2H_s}{y_{tot,mpm}} \quad (5.10)$$

where  $H_{s,lim}$  is the maximal significant wave height,  $H_s$  is the significant wave height used in the calculations, and  $y_{tot,mpm}$  is the most probable maximum value determined with the original significant wave height. The maximal significant wave height can be found for each peak period.

## 5.2 Frequency domain results

The results following from the equations given in Section 5.1 are given in this section. The most probable maximum displacements are determined for several wind and wave conditions with and without using feedback controlled taglines.

### 5.2.1 Y-compensation maxima

In Figure 5.2.1, the most probable maximum y-displacement of the blade is for a situation with and without feedback controlled taglines is shown subject to several wind and wave conditions. The maximum distance between the blade root center and the center of the hub is 0.2 m, as discussed in Section 2.5.2. The  $y_{b,mpm}$  is constantly below this maximum displacement for wave spectrum with a  $T_p$  ranging from 4 to 10 s and a wave direction from  $150^\circ$  to  $180^\circ$ , and a mean wind speed up to 10 m/s. When no feedback controlled taglines are used, the most probable maximum displacement stays below the criteria for a peak period lower than 5 s with a wave direction of  $165^\circ$  or  $150^\circ$ , or a wind speed below 8.5 m/s.

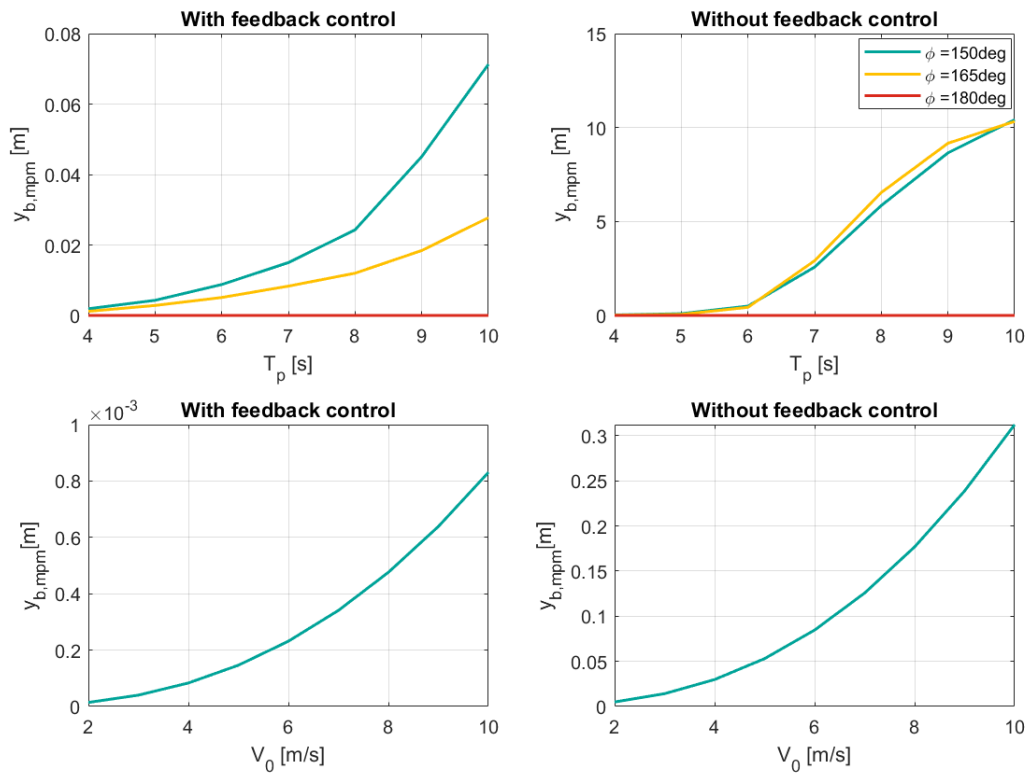


Figure 5.2.1: Most probable maximum displacement of blade root in y-direction with and without feedback controlled taglines (30-minute reference period)

## 5.2.2 $\psi$ -compensation maxima

The most probable maximum blade root displacement  $y_{br,mpm}$  due to several wind and wave conditions are given in Figure 5.2.2 for a blade with and without feedback controlled taglines. The most probable maximum displacement of the blade root does not exceed the criteria of 0.2 m for any wind speed or wave condition within the environmental envelope. When no feedback control and only a spring system is used, the maximum wind speed for which the  $y_{br,mpm}$  stays below the criteria is 3 m/s. The  $y_{br,mpm}$  does not stay below 0.2 meters for any wave condition with a wave direction of  $165^\circ$  or  $150^\circ$ . For the calculation of the blade root displacement it was assumed that the yaw angle of the blade was small. For angles smaller than  $8^\circ$ , the error of this assumption is less than 1%. For larger angles, the error due to this assumption becomes larger than 1%. For a blade root displacement larger than 3.7 m, the yaw angle of the blade is larger than  $8^\circ$ , and thus is the result not accurate anymore.

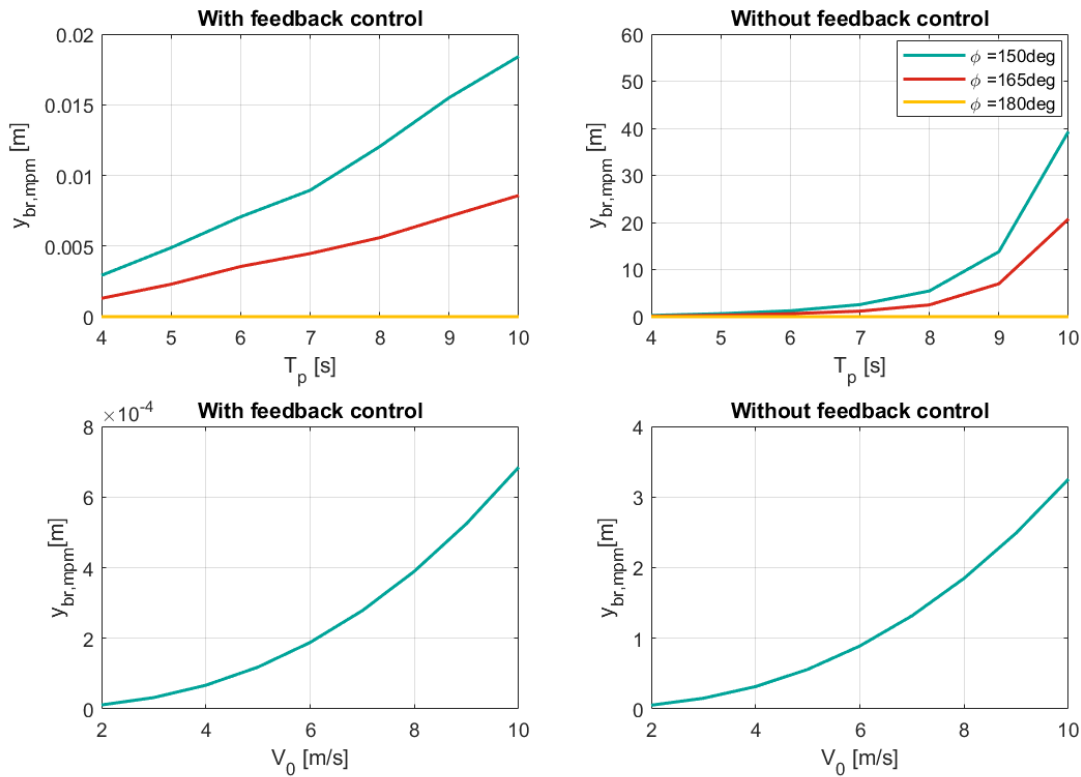


Figure 5.2.2: Most probable maximum blade root displacement  $y_{br}$  per wind and wave condition with and without feedback controlled taglines (30-minute ref. period)



### 5.2.3 Blade root displacement due to the combined force in y-direction and moment around the z-axis of the blade

The most probable maximum y-displacement of the blade root for a wave direction of  $165^\circ$  and  $150^\circ$ , a peak period of 4-10 s for the wave spectrum, and a mean wind speed of 10 m/s is shown in Figure 5.2.3. When feedback control is used, the  $y_{tot,mpm}$  values are very similar to the maximum values induced by the crane tip displacements. When no feedback control is used, the  $y_{br,mpm}$  surpasses the criteria limit with every peak period of the waves. This is caused by the 10 m/s wind speed, which already induces a blade root displacement of 3.2 m.

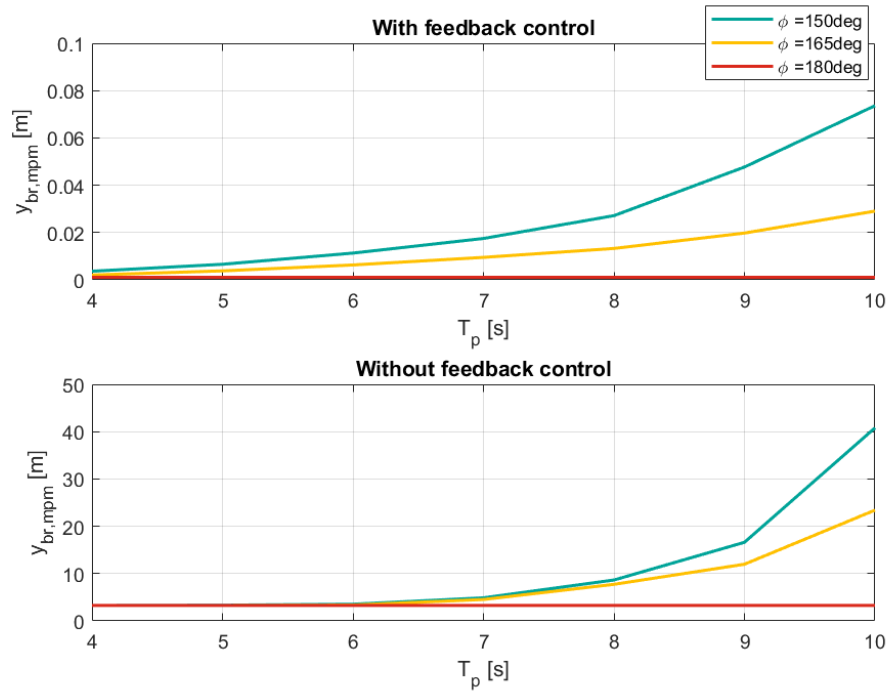


Figure 5.2.3:  $y_{br,mpm}$  per wave direction, wave peak period, and with a mean wind speed of 10 m/s (30-minute ref. period)

### 5.2.4 Operational limits

By applying Equation 5.10 on the  $y_{tot,mpm}$ , found by applying a wind environment with a mean wind speed of 10 m/s and varying wave loads, the limiting wave height can be found for each peak period. The limiting significant wave height for peak periods equal or below 8 s or with a wave direction of  $165^\circ$ , are larger than 14.7 m. High waves with a relatively short period will induce non-linear wave loads not considered within linear theory. For a wave angle of  $\psi = 150^\circ$ , and a peak period  $T_p$  of 9 and 10 s, the limiting significant wave heights are respectively 8.4 m and 5.4 m.

## 6 | Time domain model

To include the non-linearities of only pulling the taglines and to the coupling terms of the blade motions, two time domain simulations needs to be done. The time domain model is made in aNySIM, the general theory behind the software is explained in Section 6.1. An overview of the input and output values of the model is given in Section 6.2. The model is verified by doing several load cases and comparing the RAOs of the vessel to the RAOs from the WAMIT data. This verification is discussed in Section 6.3. The modeling of the taglines is a separate submodel, the numerical modeling of the taglines is discussed in Section 6.4. A selection of the results of the simulations are given in Section 6.6.

### 6.1 General theory behind aNySIM

The time domain simulations are done using the software aNySIM, a program developed by MARIN (Maritime Research Institute the Netherlands). This software is developed for analysis of multibody dynamics in offshore operations.

Classically, ship motions are calculated with Equation 6.1. The ship motions are assumed to be harmonic, with a frequency dependent added mass  $a_{kj}$ , and a frequency dependent damping coefficient  $b_{kj}$ . In aNySIM the non-linear responses are also considered, which means the simple mass-damper-spring analysis cannot be used.

$$\sum_{j=1}^6 (M_{kj} + a_{kj}) \ddot{x}_j + b_{kj} \dot{x}_j + c_{kj} x_j = F_k \quad \text{with } k, j = 1, 2 \dots 6 \quad (6.1)$$

To include the non-linear effects the impulse response theory is applied, resulting in Equation 6.2, where  $m_{kj}$  is the frequency independent added mass, and the  $R_{kj}$  the retardation function. The  $F_k$  includes all arbitrarily in time varying external forces.

$$\sum_{j=1}^6 (M_{kj} + m_{kj}) \ddot{x}_j + \int_{-\infty}^t R_{kj}(t - \tau) \dot{x}(\tau) d\tau + c_{jk} x_j = F_k(t) \quad \text{with } k, j = 1, 2 \dots 6 \quad (6.2)$$

The relation between the frequency domain and the time domain quantities are as followed:

$$a_{kj} = m_{kj} - \frac{1}{\omega} \int_0^{\infty} R_{kj}(t) \sin \omega t \, dt \quad (6.3)$$

$$b_{kj} = \int_0^{\infty} R_{kj}(t) \cos \omega t \, dt \quad (6.4)$$

The retardation functions and the coefficients of added inertia can be derived by taking the inverse Fourier-transform of Equation 6.3 and 6.4. This means that, at one frequency, the  $R_{kj}$  and  $m_{kj}$  can be derived from the frequency dependent coefficients:

$$R_{kj}(t) = \frac{2}{\pi} \int_0^{\infty} b_{kj}(\omega) \cos \omega t \, d\omega \quad (6.5)$$

$$m_{kj} = a_{kj}(\omega') + \frac{1}{\omega'} \int_0^{\infty} R_{kj}(\tau) \sin \omega' \tau \, d\tau \quad (6.6)$$

Three different time simulation solvers can be used for simulation: Heun Runge-Kutta (RK2), Runge-Kutta 4 (RK4), and Cash-Karp (RK45). The accuracy and stability of the computed  $\mathbf{y}(t_1)$  is improved by using more derivations of function  $\mathbf{f}$ . With RK2, the average of two derivatives is used to estimate  $\mathbf{y}(t_1)$ . In RK4, four derivatives are used, and in RK45 six derivative functions are used. Each derivation takes time in to simulate, hence, solving with RK45 is three times slower than RK2. However, the RK45 is usually more precise and has a larger stability range.

## 6.2 Overview aNySIM model

The input values for the model are:

1. The hydrodynamic data generated by WAMIT
2. Vessel properties
3. Environmental conditions, the environmental window is discussed in Section 2.3.
4. Blade information
5. Taglines and control systems
6. Solver settings

Finding the y-motions of the blade is the final goal of the model, the motions of the vessel and the blade in 6DOF are determined using the input values mentioned above. The simulations are run for two wave directions:  $165^\circ$  and  $150^\circ$ . Since there are two non-linearities to take into account, the simulations are run with taglines which can exclusively pull, and with and without constraints on the x-displacement of the blade.

To compare the results with and without constraints on the x-direction of the blade, the same randomness seed is used for each simulation. The randomness seed determines the random phase angle of the wind and waves. By using the same randomness seed, the results are not influenced by having a different statistical distribution of the phase angle.

## 6.3 Model verification

The vessel model needs to be verified with the load cases listed below. The principle of each load case is explained and the outcome is compared to the results from the frequency domain analysis. Since the non-linearity of the total model will be in the tagline system, there should be minimal differences between the frequency and time domain calculation results in these load cases.

1. Still water load case
2. Static heel and decay load case
3. RAO comparison with frequency- and time domain determined vessel motions

After verifying the vessel model, the blade model and wind loads need to be verified, this is described in the last paragraph of this section.

### 6.3.1 Still water load case

In the still water load case, the vessel hull is simulated in still water. The hull should have no motion in the water, since there are no waves and no other external forces. The test is successful if the body does not have any initial motion. The center of gravity (CoG) of the vessel, the mass and the displacement are checked through this test. The data on the vessel is given in Appendix A.

### 6.3.2 Static heel and decay load case

The natural period of the vessel model in roll and pitch, and the metacentric height in longitudinal and transverse direction are tested in the “Static heel and decay load case”. A constant moment is applied around the vessel x-axis to which the body will find a static roll angle. After some time the moment is removed and the body will go back to its original position. After finding its equilibrium position, the body will decay with its natural roll frequency. The same is done for the y-axis to find the static pitch angle and the natural pitch frequency. The heel angle and natural period resulting from the load case, the analytical data, and the difference between the two, are given in Table 6.3.1. The analytical results and model results are approximately equal.

Table 6.3.1: Analytical and load case model results of static heel and decay test

	Analytical	Model result	Difference
T44 [s]	12.7	12.8	0.08%
T55 [s]	10.6	10.7	0.1%
Static roll angle [°]	4.12	4.12	0.0%
Static pitch angle [°]	0.305	0.309	1.3%

### 6.3.3 RAO comparison with frequency- and time domain determined vessel motions

The wave response of the vessel model can be checked by comparing the frequency- and time domain determined response amplitude operator (RAO) of the six degrees of freedom of the vessel. The RAOs determined in frequency domain are obtained using analytical expressions and the hydrodynamic data from WAMIT. The RAOs determined from the time domain model are obtained by use of a white noise spectrum and taking the Fourier transform of the simulation.

The RAOs of the 6DOF of the vessel obtained for a wave heading of  $165^\circ$  and  $180^\circ$  are given in Figure 6.3.1 and 6.3.2, in both figures the RAOs from the frequency domain calculations are also given. The wave heading is defined as shown in Figure 2.3.1. To bring the RAOs in perspective the wave peak period  $T_p$  of 4-10 s, that will be considered later in the research, is highlighted in the figures.

Several differences can be noted between the time domain calculated RAOs and the frequency domain determined RAOs.

- For the surge motion in x-direction, the peak of the frequency domain is higher than the time simulations peak. This is mainly due to the inaccuracy of calculating the influence of waves with a very long wave period on the vessel. Very long waves approach a still water environment. The effect of long waves in a time domain simulation therefore approach zero, while theoretically the effect keeps rising the closer the wave frequency comes to 0 rad/s.
- The sway motion in y-direction is approximately zero for all frequencies for a wave heading of  $180^\circ$ . For a wave heading of  $165^\circ$  it is visible that the vessel motions fast increase when the frequency gets below 0.2 rad/s.
- The heave motion curves of the frequency and time domain calculations are very similar. The main difference is that the time domain curve does not start at 1. This is due to the inaccuracy with frequencies near zero where
- The yaw motion RAO is very small for a wave heading of  $180^\circ$ , both equal to zero m/m for all frequencies. For a wave heading of  $165^\circ$  the expected yaw motion is non-zero, in the time simulations the yaw-motion has a different RAO than the frequency domain determined RAO. A natural frequency is visible in the RAO in time domain. This natural frequency is caused by a rotational spring that was added to the vessel to resemble a DP-system. A DP-system will also have a low-frequent natural frequency, hence, the natural frequency stays in the time domain model.

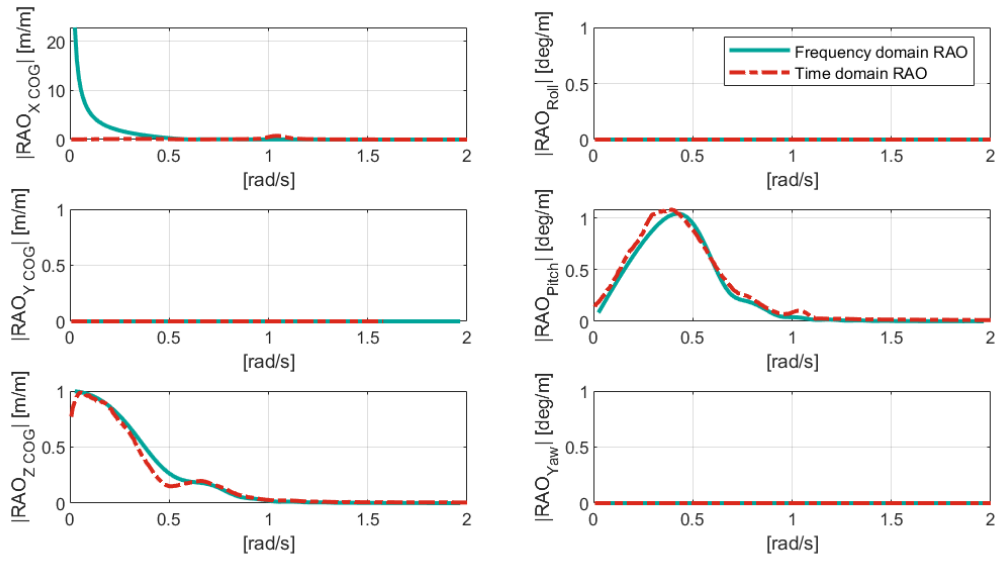


Figure 6.3.1: RAOs determined in frequency domain and by time simulations of the 6DOF of the vessel with a wave heading of  $180^\circ$

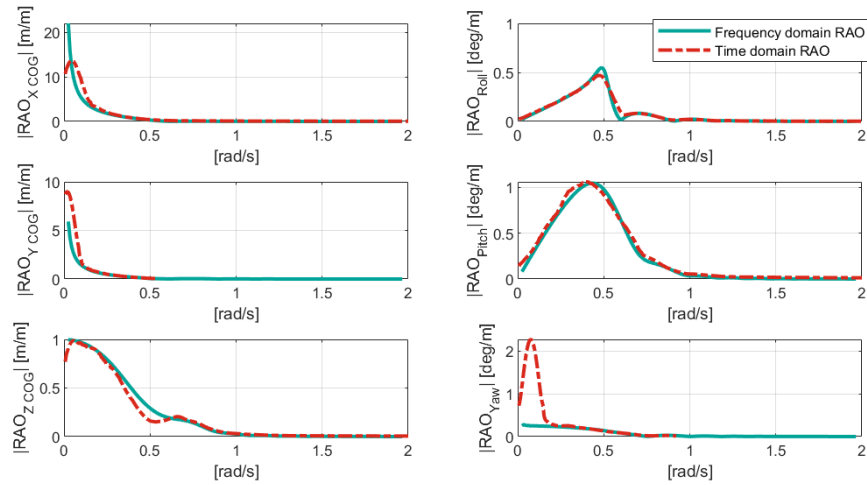


Figure 6.3.2: RAOs determined in frequency domain and by time simulations of the 6DOF of the vessel with a wave heading of  $165^\circ$

### 6.3.4 Blade model verification

The blade model can be verified by plotting the wind induced moment on the blade according to the frequency domain calculations and the Fourier transform of the time domain model. The spectrum of the wind induced moment on the blade determined in time and frequency domain is shown in Figure 6.3.3. As can be seen, the spectra are very similar.

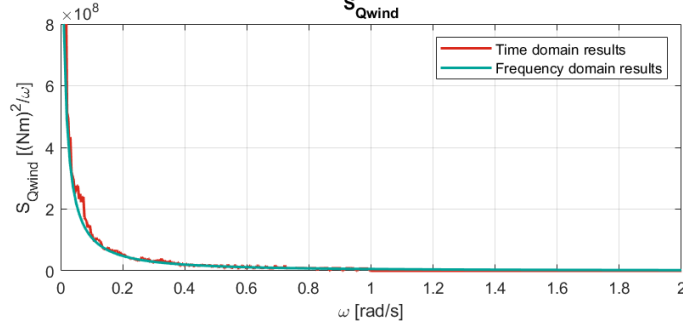


Figure 6.3.3: Spectrum of wind induced moment on the blade with a mean wind speed of 6 m/s

## 6.4 Tagline modeling

In the aNySIM software, there is no standard way to model the PID-controlled taglines. A submodel is made to include the PID-controlled taglines in the model. This numerical submodel is made in Python; it calculates the forces on the blade for each time step.

The tagline forces are calculated based on the error, time derivative of the error, and the integral over the past errors of the y-displacement and  $\psi$ -angle of the blade. Both the taglines carry half of the force needed for compensation in y-displacement. They also both provide for half of the needed moment to compensate for the  $\psi$ -displacement. The integral over the error is determined over the last 20 seconds of the simulation. The tagline forces are determined with:

$$F_{tl,i} = \frac{1}{2}F_{y,i} \pm \frac{1}{l_{bg}}M_{\psi,i} \quad (6.7)$$

$$F_{y,i} = (y_i - y_{ref})k_{py} + \sum_{j=i-20sec}^{j=i} ((y_j - y_{ref})\Delta t)k_{iy} + \frac{y_i - y_{ref}}{\Delta t}k_{dy} \quad (6.8)$$

$$M_{\phi,i} = (\psi_i - \psi_{ref})k_{p\psi} + \sum_{j=i-20sec}^{j=i} ((\psi_j - \psi_{ref})\Delta t)k_{i\psi} + \frac{\psi_i - \psi_{ref}}{\Delta t}k_{d\psi} \quad (6.9)$$

where  $i$  is the current time step,  $F_{y,i}$  is the needed force to compensate for the y-displacement,  $l_{bg}$  is the length of the blade gripper,  $M_{\psi,i}$  is the needed moment to compensate for the  $\psi$ -displacement,  $y_i$  and  $\psi_i$  are the current y- and  $\psi$ -position of the blade,  $y_{ref}$  and  $\psi_{ref}$  are the reference y- and  $\psi$ -position of the blade,  $\Delta t$  is the time step of the time simulation,  $k_{py}$ ,  $k_{iy}$ , and  $k_{dy}$  are the PID-controller gains for the controller for the blade y-position, and  $k_{p\psi}$ ,  $k_{i\psi}$ , and  $k_{d\psi}$  are the PID-controller gains for the controller for the blade  $\psi$ -position.

### 6.4.1 Saturation check

The taglines can only adjust a pulling force on the blade; the minimum force of a tagline is  $F_{min} = 0$  N. The maximum applicable force is dependent on the winch limitation. Assuming the winches can provide enough torque and torque-speed, the maximum force is neglected. When the demanded pulling force from the controller is smaller than 0 N, the output will saturate at 0 N until the force increases again.

### 6.4.2 Anti-windup

Anti-windup is a feature that prevents the integral error from building up after the minimum, or maximum force is reached. For example, when the blade error is negative, the integral error  $\sum_{j=i-20sec}^i ((y_j - y_{ref})\Delta t)$  will keep decreasing whilst the taglines are no longer providing any force. When the line can pull the blade again, the integral has increased so much that the pulling force will stay at 0 N until the error has been positive for a longer time.

In the tagline submodel, the anti-windup is applied with a method called clamping. The clamping ensures that the controller force due to the integral is off when saturation at the  $F_{min}$  occurs. It consists of two steps:

1. When the PID-controller gives an output which is smaller than  $F_{min}$ , the output is set to zero by the saturation check. The first check of the clamping system is to see if the input and output of the saturation check are equal. If they are, saturation took place; if they are not, no saturation took place.
2. The second check is to see if the sign of the output of the PID-controller is equal to the sign of the error; if so, the integrator is still adding to the output making the controller output more negative and thus attempting to add pushing force.

When both of these checks are positive, saturation is happening, and the integrator is attempting to make it worst, the  $k_i$  is set to zero until the outcome of either step is not positive anymore.

## 6.5 Model description

The maximum blade root displacement is determined for the wind and wave conditions described in Section 2.3. The time simulations are 30-minute long, with a run-up time of 200 seconds. The maximum blade root displacements are firstly determined with wave loads acting on the vessel, then with wind loads working on the blade, and finally with both wind and wave loads.

In each time series, the same randomness seed is used for the random phase of the waves and wind. However, different time series are run to investigate the influence of the randomness seed on the maximum blade root displacement by changing the randomness seed in the input of the time simulation. The randomness seed changes the wave elevation's random phase angles and the phase angles of the varying part of the wind. The outcome is dependent on these variations. Hence, to determine the reliability of the results of the performed time simulations, the influence of the randomness seed on the results should be investigated. This is done by comparing the results of multiple different time simulations with the same environmental conditions and a different randomness seed. The maximum blade root displacement  $y_{br,m}$  is determined for ten different randomness seeds. The



two situations that are investigated are the following two sets of environmental conditions:

Case 1:  $T_p = 10$  s,  $\phi = 150^\circ$ ,  $V_{10} = 10$  m/s, 3m predisplacement

Case 2:  $T_p = 6$  s,  $\phi = 150^\circ$ ,  $V_{10} = 10$  m/s, 2m predisplacement

To check the estimation of the winch capacity made in Section 3.2.3, the maximum torque and torque speed is derived for three cases. The three cases are:

Case 3:  $T_p = 10$  s,  $\phi = 150^\circ$ ,  $V_{10} = 10$  m/s, 3m predisplacement

Case 4:  $T_p = 10$  s,  $\phi = 150^\circ$ ,  $V_{10} = 10$  m/s, 2m predisplacement

Case 5:  $T_p = 9$  s,  $\phi = 150^\circ$ ,  $V_{10} = 10$  m/s, 2m predisplacement

## 6.6 Results time domain simulation

The results following the 30-minute time simulations of the mating phase are given in this section. The maximum blade root displacement in y-displacement due to several waves and wind loads are given. First, the results due to wave loading are given, then the results due to wind loading are given, and then the combined wind and wave load results are given.

### 6.6.1 Blade root displacement due to wave loads

The maximum values for sea states with  $H_s = 2$  m, and  $T_p$  of 4, 6, 8, 9, and 10 s, and a wave direction of  $150^\circ$  and  $165^\circ$ , are shown in Figure 6.6.1. The pretension on the blade caused the blade to displace 2m; however, for the run with a wave direction of  $150^\circ$  and a peak period of 10 s, the crane tip displaced more than 2 meters. To find the maximum blade root displacement for a situation where the predisplacement of the blade is larger than the maximum crane tip displacement, another run was done with a blade predisplacement of 3 meters.

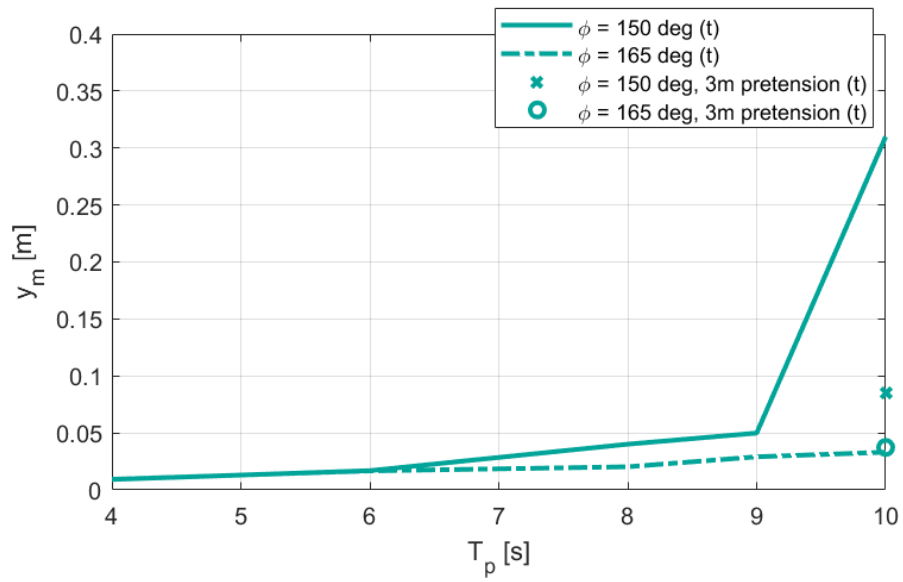


Figure 6.6.1: Maximum y-displacements per sea state

### 6.6.2 Blade root displacement due to wind loads

The maximum values of the y-displacement of the blade root, subjected to wind loads with a mean wind speed of 2-10 m/s from a 90° wind angle, are shown in Figure 6.6.2. Looking into the time simulations, it can be seen that the main displacement due to the wind loads is caused by the yaw motion of the vessel, which results in an angle of the blade in the global axis system. The  $RAO_{zeta, \psi_s}$  has a natural period at 0.1 rad/s due to the spring added to the system. The wind loads on the blade are compensated by the tagline forces, which work in the opposite direction on the crane boom. These wind compensating forces are working with the natural frequency of the yaw motion, which causes the vessel to yaw.

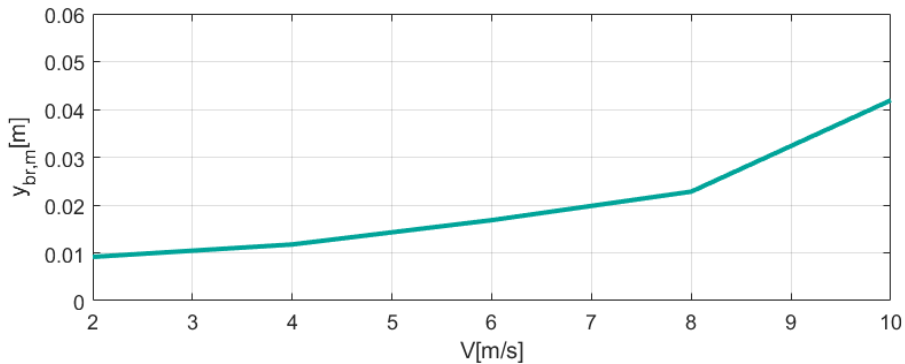


Figure 6.6.2: Maximum y-displacement of blade root per mean wind speed

### 6.6.3 Blade root displacement due to combined wind and wave loads

The maximum displacement with a wind speed of 10 m/s is 0.042 m. To investigate the combined impact on the blade motion, the system is subjected to wind and wave loads simultaneously. The wave direction is 150°, the peak period ranges from 4-10 s, and the mean wind speed is constant at 10 m/s from a 90° angle. In Figure 6.6.3 the maximum y-displacements of the blade root for only the wave loads and the situation with both wind and wave loads are given. The results are also given with a predisplacement of 3 meters for the situation with a peak period of the wave spectrum is 10 s.

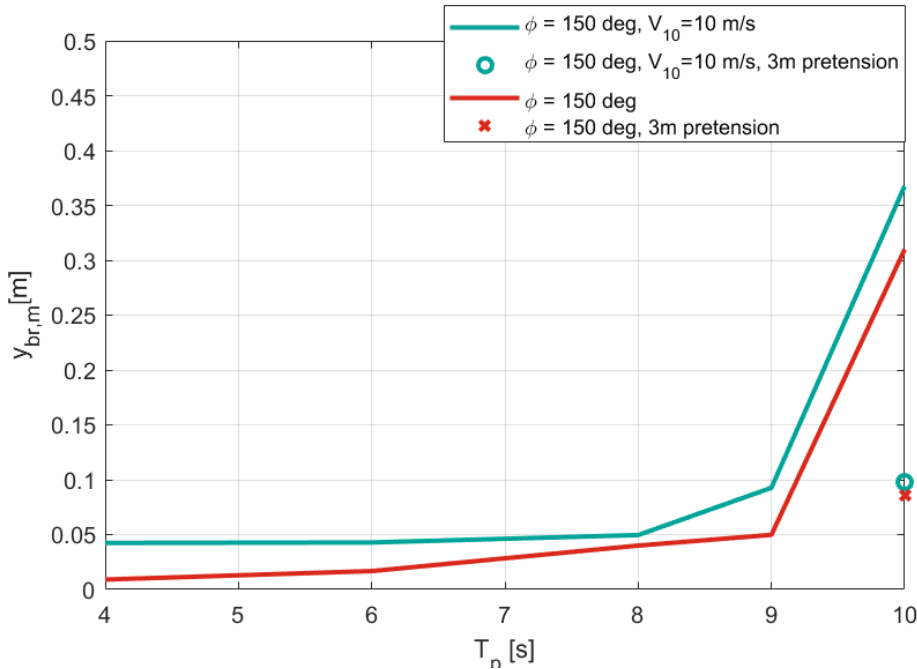


Figure 6.6.3: Results for maximum blade root y-displacement with simultaneously simulated wind and wave loads, the mean wind speed is 10 m/s, the wave direction is  $\psi=150^\circ$ , the results plotted per peak period of the wave excitation spectra

#### 6.6.4 Randomness seed variation

The maximum blade root displacement  $y_{br,m}$  for ten different randomness seeds are displayed in Table 6.6.1. For case 1, the maximum blade root displacements range from 0.08 m to 1.70 m. This means that for some cases, the blade root displacement stayed below 0.2 m, and for others, it went over the criteria. Looking into time serie 6 of this case, it was visible that the crane tip had a displacement of over 3 meters at a certain time and the taglines lost tension. In cases 1, 3, 5, and 9, one tagline lost tension at some point during the time simulation, which resulted in a higher displacement of the blade root. All the results of the second case range between 0.039 and 0.043 meters, and the taglines never lose tension. The results are further discussed in Section 7.2.

Table 6.6.1: Maximum blade root displacements for two different sets of environmental conditions with ten different randomness seeds

Number [#]	1	2	3	4	5	6	7	8	9	10
Case 1 $y_{br,m}$ [m]	0.42	0.09	0.19	0.08	0.18	1.70	0.11	0.09	0.23	0.10
Case 2 $y_{br,m}$ [m]	0.038	0.039	0.042	0.043	0.041	0.040	0.039	0.039	0.043	0.043

### 6.6.5 Winch capacity

When a winch diameter of 1 meter is assumed, the maximum torque and torque speed of the winches can be determined using the maximum force required to compensate for the blade motions for the two cases. These values are shown in Table 6.6.2. The results are further discussed in Section 7.2.

Table 6.6.2: Needed winch capacity

Case	$Q_{max}$ [kNm]	rpm [rpm]
3	260	5.6
4	215	5.6
5	170	3.2

# 7 | Analysis of frequency and time domain results

In this chapter, the results from the frequency domain calculations in Section 5.2 and the time domain simulations in Section 6.6 are compared in Section 7.1 and the differences are discussed in Section 7.2.

## 7.1 Analysis and comparison of results

The results from the frequency domain (FD) calculations and time domain (TD) simulations are compared in this section. First, the impact of waves will be discussed, then the difference in wind influence, and last, the results due to combined wind and wave loading.

### 7.1.1 Wave load impact, time- and frequency domain result

To compare the results of the FD and TD calculations, they are plotted in one figure. The most probable maximum y-displacement of the blade with varying sea states with a 30-minute reference period determined in the FD and the maximum y-displacement of the blade in a 30-minute TD simulation are shown in Figure 7.1.1. As can be seen, the results of the FD and TD calculations are close to each other. The difference between the TD and FD results stays approximately the same when the peak period of the wave spectrum increases for a wave direction of  $165^\circ$ . The TD results are at each peak period a bit higher than the FD results. For a wave direction of  $150^\circ$ , the difference at a wave peak period of 10 seconds is very large when only 2 m predisplacement is used. The results of TD and FD are close together when 3 m predisplacement is used. When the crane tip displacement is greater than the predisplacement of the blade, the taglines lose tension, and thus, the blade motion is not controllable anymore. With a larger predisplacement, the taglines stay under tension, and thus the displacement of the blade in y-direction stays below the criteria.

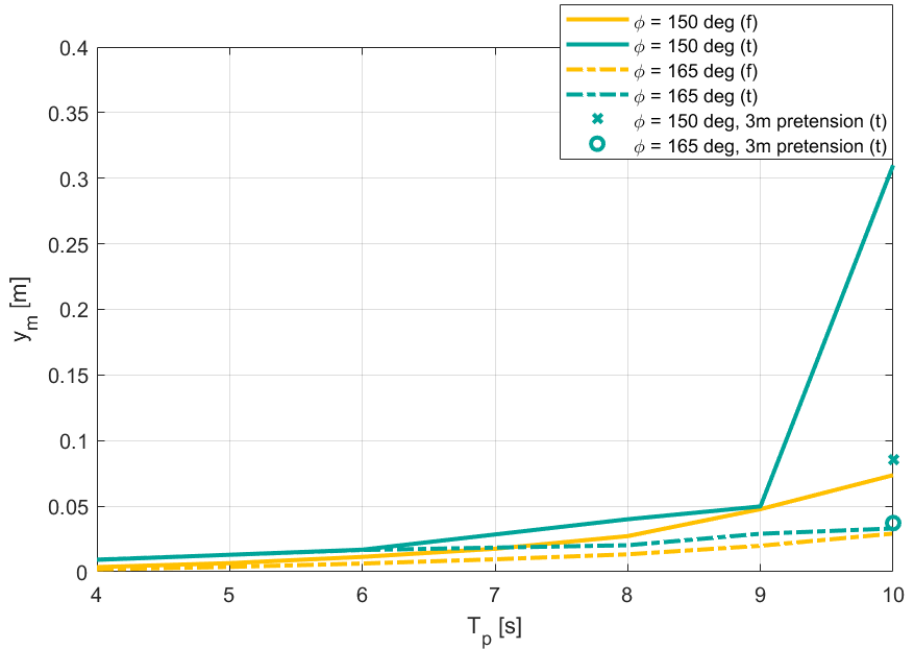


Figure 7.1.1: Y-displacement of blade root in frequency (f) and time (t) domain due to wave loads

### 7.1.2 Wind load impact, time- and frequency domain result

The most probable maximum blade root displacement due to wind loads with a mean wind speed of 2 to 10 m/s for a 30-minute reference period resulting from the FD calculations and the maximum blade root displacement in TD simulations of 30-minutes are displayed in Figure 7.1.2.

There is a significant difference between the FD-determined most probable maximum displacement of the blade root and the maximum blade root displacement resulting from the TD simulations. The blade root displacement resulting from the FD calculations is approximately zero, while the blade root displacement reaches up to 0.04 m for a mean wind speed of 10 m/s in the TD simulations.

### 7.1.3 Impact of wind and wave loads time vs. frequency domain result

The results of the combined wind and wave loads for the FD calculations and TD simulations are displayed in Figure 7.1.3. A constant mean wind speed of 10 m/s is used in each calculation. The maximum blade root displacement of the TD simulations with a wave peak period of 4 - 8 s stays constant at 0.042 m, which is the maximum displacement for a mean wind speed of 10 m/s. Again, the TD  $y_{br,m}$  becomes significant for a wave peak period of 10 s when the predisplacement is 2 m because the taglines lose tension. The TD  $y_{br,m}$  for a predisplacement of 3 m is near to the FD determined results.

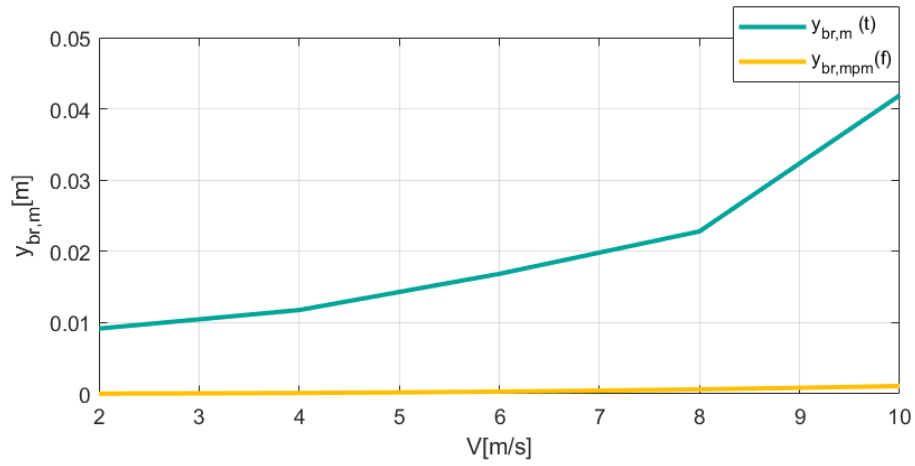


Figure 7.1.2: Y-displacement of blade root in frequency- (f) and time- (t) domain due to wind loads, per mean wind speed between 2-10 m/s

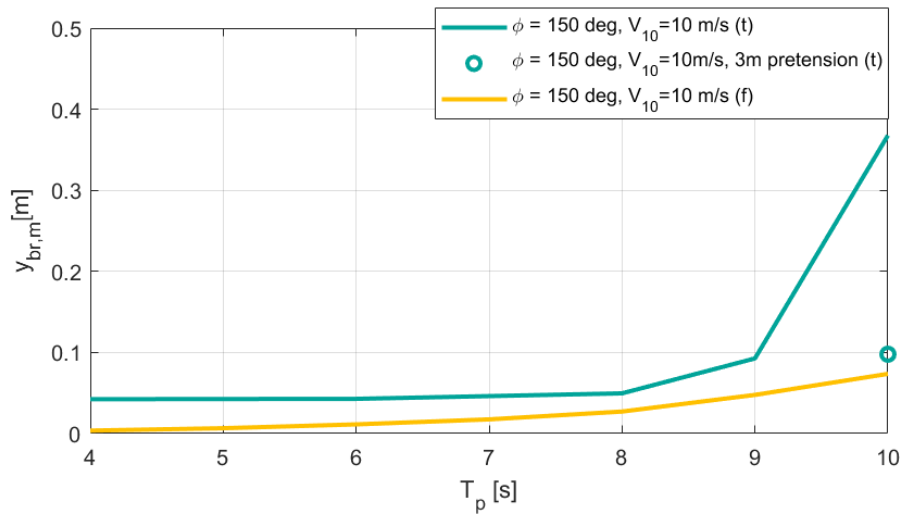


Figure 7.1.3: Y-displacement of blade root in frequency (f) and time (t) domain due to wind with  $V_{10} = 10 \text{ m/s}$ , and varying wave loads



## 7.2 Observed differences discussion

In the calculations and simulations with only wave loads, the TD results are not far off the FD calculated  $y_{b,mpm}$ . The  $y_{b,mpm}$  is a statistical value; hence, it is expected that one time simulation with random phase periods will not have the same maximum displacement. However, the TD results are consistent with a constant distance above the FD result. The yaw-motion of the vessel causes this difference. The yaw-motion of the vessel has a natural frequency at 0.1 rad/s in the TD simulations. In FD, the yaw-motion of the vessel does not have this natural frequency. Hence, this motion has a minor influence on the results. The taglines can only pull in TD, while they can apply any force in FD. This is only noticeable in the result caused by the wave spectrum with a peak period of 10 s; there, the resulting y-displacement shoots up to 0.31 m. When a larger predisplacement is applied on the blade, the result is again on the expected position.

When wind loads are applied to the blade, the blade root displacements in TD are higher than the FD results. This is also caused by the yaw-motion of the vessel. In TD, the tagline forces working on the blade work in the opposite direction on the crane boom. The fluctuating part of the wind speed works at a low frequency, and the natural frequency of the vessel yaw-motion is 0.1 rad/s. Thus, the wind compensation forces are exciting the vessel's natural frequency in yaw-direction.

When the wave and wind loads are simultaneously working on the body, the mean wind speed is 10 m/s in each simulation. For a wave peak period of 4 to 8 s, the maximum displacement in TD stays constant at the same value as when only the wind loads would be applied. The blade root displacement grows when the waves have a wave peak period of 9 and 10 s. All results are higher than the most probable maximum calculated in FD. This is mainly caused by the difference in response to the wind loads. Since the response is approximately zero for the wind loading in FD, the wind has little influence on the FD results. The TD results show that the maximum blade root displacement is not equal to the summation of the displacement due to wind and wave loading. The maximum blade root displacement stays equal to the maximum displacement due to wind loading until the wave-induced maximum displacement surpasses the wind-induced maximum.

The randomness seeds were investigated for two cases in the combined wind and wave simulation in Section 6.6.4. The outcomes at a peak period of  $T_p = 6$  s were always close to 0.04 m, while the results for a peak period of  $T_p = 10$  s were far apart. Based on these findings, it can be concluded that the randomness seed can only make a big difference when the pretension is not larger than the maximum crane tip displacement. When the needed predisplacement of the blade is determined prior or during an operation, a margin should be build-in between the expected maximum crane tip displacements and the predisplacement of the blade to secure safe installation.

The maximum required winch capacity for three cases are stated in Section 6.6.5. What can be concluded from these results is that the winch capacity is dependent on the pretension that is applied on the blade. However, the maximum predisplacement of the blade is limited by the position and angle of the crane boom, since collision between the blade and the crane boom must be avoided. Since the crane boom of the EnsysXL is very tall, it can be assumed that enough space can be created between the blade and the crane boom for a predisplacement of 2 to 3 meters. For a predisplacement of 3 meters, the maximum required torque is 260 kNm and the maximum winch speed is 5.6 rpm, assuming a winch radius of 1 m.

What should be noticed is that, when the pretension is large enough, all y-displacements for combinations of wind and wave loading are under the 0.2 m maximum displacement. However, the criterion for installation is a circle with a radius of 0.2 m. So whether the blade root center stays within the 0.2 m radius circle is also dependent on the displacement in the z-direction. According to the results, the y-displacement stays below 0.1 m, meaning the z-motion of the blade root could have a maximum displacement of 0.17 m.



## 8 | Discussion

Several assumptions were made in this project. Some of these assumptions will have had a more significant effect on the project results than others. In this chapter, several assumptions are discussed and questioned.

### **The tagline coupling forces**

The tagline forces are assumed to be directed in the y-direction of the blade. However, when the blade has motion in the x-direction, the taglines apply a vector force in y- and x-direction. This would mean the forces determined by the feedback controller would not only be directed in the y-direction and thus would not compensate the blade motions as it should. The same can be argued for the blade motion in the z-direction. The blade motion in x-direction would also be excited due to the angle of the taglines; this could cause possible instability.

### **Coupling of the three compensation systems**

In the proposed lifting concept, three compensation systems are simultaneously at work. In this project, one of the compensation systems for y- and yaw-compensation is researched. The blade's x- and pitch-motion are assumed to be fully compensated by the blade gripper and the taglines to the crane tip. The compensation in the z-direction is not applied yet. The y- and yaw-compensation performance might be affected when the other two compensation systems are also at work. The combined stability and performance are not considered in this research.

### **No measurement noise or errors**

Assuming the sensors of the feedback system can detect any motion perfectly and send it to the controller without any noise or errors is a large assumption to make. The measurements of the blade motions must be exact since the maximum displacement of the blade root is only 4% of its diameter. If an error is made in the measurements, the feedback system will apply a fault force on the blade, and the blade root displacement might become worse.

### **A rigid crane**

The crane tip in this project has to be at least 175 meters high. Even though the Ensyst XL crane is placed on a pedestal of 80 m, the crane boom will still have some flexibility. The crane's flexibility will not significantly influence the working of the tagline compensation system since the displacement of the crane tip is modeled as an unspecified disturbance. Hence, if the crane tip

motion varies from the rigid body motion due to the crane flexibility, this will not affect the control system of the blade.

## 9 | Conclusion

In this thesis, the operational limits of a single blade installation with a floating monohull crane vessel were sought. An installation method was proposed to install a single blade to the turbine hub using a floating crane vessel and three separate control systems to limit the motions of the blade. The control system minimizing blade motions induced by the roll motions of the vessel has been investigated in more detail, as compensation in this degree of freedom was considered to be most critical. In this compensation system, the position of the blade is controlled with two dynamically controlled taglines towards the crane boom. The operational limits that needed to be determined are based on the last phase of installation; the mating phase. During the mating phase, the typically accepted motion limit is 0.2 m between the blade root center and the hub center, which means the blade has a small motion window.

Both the wind- and wave-induced blade motions have been considered. The control parameters were determined based on the equations of motion of the blade, and the wind- and wave-disturbances. The installation was modeled to find the operational limits during the mating phase. Several of the most important assumptions that were made are:

- First order potential flow is used to determine the wave loading on the vessel.
- Rigid body motions are assumed for the vessel, crane, and blade body.
- The two compensation systems that are not modeled in detail are assumed to work. Hence, the blade motions in these directions are assumed to be zero.
- No measurement noises are considered in the feedback loop of the tagline control system.

The modeling of the installation has been performed in both the frequency and time domain. The latter model has been made to investigate the impact of some non-linearities, which could not be effectively modeled in the frequency domain. The main conclusions resulting from the models are:

- When the blade can only be pulled and not pushed by the taglines, there is no great consequence for the displacement of the blade root if the crane tip motions stay below the predisplacement of the blade towards the crane boom. The randomness sensitivity study showed that a margin should be build-in between the expected maximum crane tip displacements and the predisplacement of the blade to secure safe installation.
- The frequency domain calculated most probable maximum blade root displacement lies 1 to 3 cm lower than the results from the time domain simulations when the pretension on the

blades is larger than the maximum crane tip displacement. The biggest difference between the results from frequency and time domain is due to the yaw-motions of the vessel.

- When the operational limits of the installation are determined with linear theory, a feedback system is capable of compensating for the blade motions in  $y$ -direction for an extensive range of environmental conditions. If limiting the wave direction to an interval of  $150\text{-}210^\circ$ , the control system can limit the  $y$ -motions at the blade root below 0.2 m, up to a wave height of  $H_s = 5.6$  m and  $T_p$  of 10 s.
- The maximum winch capacity to displace the blade 3 meters towards the crane boom and operate with a sea state of  $H_s = 2$  m,  $T_p$  of 10 s, and wave direction of  $150^\circ$  is 260 kNm with a winch speed of 5.6 rpm.

To make a more accurate estimation of the operational limits, it is recommendable to include the other two compensation systems in the model, include the taglines in the model as actual spring-like lines instead of point loads, and investigate possible coupling effects between the compensation systems.

## 10 | Recommendations

In this project, the operational limits for a single blade installation with a monohull crane vessel are sought. A concept lifting method is proposed and used to determine the maximum displacement of the blade root in y-direction while being controlled by feedback-controlled taglines. Recommendations for future research related to this project are:

- In this project, the focus was on compensating the blade motions in the y-direction. The compensation of blade motions in x-, and z-direction should be investigated in order to make a better estimation of the operational limits.
- When all three compensation systems are used, coupling forces will most probably occur between the compensation systems. The effect of these coupling effects should be researched, and possibly a decoupling strategy must be found.
- In this project, the tagline forces are modeled as point forces in the y-direction. If the blade has a motion in the x-direction, the taglines work under an angle, and thus, the taglines will apply a force on the blade in x- and y-direction. The force in x-direction is not considered in this project. In further research, the coupling terms of the taglines should be determined.
- Since the blade root stays below the motion criteria in this criteria. Research should be done to investigate the influence the size of the ship has on the operational limits.
- The sensors are assumed to work perfectly. Research should be done to determine the effect of errors and noise in the feedback loop on the system's performance.





# Bibliography

- [1] O. Edenhofer. The IPCC Special Report on Renewable Energy Sources and Climate Change mitigation. September 2011.
- [2] D. Ahn, S.-C. Shin, S.-Y. Kim, H. Kharoufi, and H.-C. Kim. Comparative evaluation of different offshore wind turbine installation vessels for Korean west-south wind farm. *International Journal of Naval Architecture and Ocean Engineering*, 2016.
- [3] Fred. Olsen Windcarrier. Case Study: Alstom Haliade Demonstrator. url: <https://windcarrier.com/alstom-haliade-demonstrator-9>.
- [4] P. Guillen and N. Wetzler and N. Abstoss. Analysis of Maryland Port Facilities for Offshore Wind Energy Services. 2011.
- [5] Nadja Skopljak. Arcadis Ost 1 First to Use Floating Turbine Installation Method. *www.offshorewind.biz*, November 2019.
- [6] Temporary Work Design. Blade Installation Tool. url: <https://twd.nl/solutions/innovations/blade-installation-tool/>.
- [7] Lagerwey. CLIMBING CRANE – LCC140. url: <https://www.lagerwey.com/climbing-crane/>.
- [8] Det Norske Veritas AS. Marine operations, general. (Section 4 - B):28–33, 2011.
- [9] J.M.J. Journée and W.W. Massie. *Offshore Hydromechanics*. Delft University of Technology, 2001.
- [10] O.M.Faltinsen. *Sea loads on ships and offshore structures*. Cambridge University Press, 1990.
- [11] E. Gaertner, J. Rinker, L. Sethuraman, F. Zahle, B. Anderson, G. Barter, N. Abbas, F. Meng, P. Bortolotti, W. Skrzypinski, G. Scott, R. Feil, H. Bredmose, K. Dykes, M. Shields, C. Allen, and A. Viselli. Definition of the IEA 15-megawatt offshore reference wind turbine. Technical report, International Energy Agency, 2020.
- [12] I. Komusanac, G. Brindley, and D. Fraile. Wind energy in Europe in 2019 - Trends and statistics. *Wind Europe*, February 2020.
- [13] IEA. Planned 2020 investments in upstream oil and gas have been slashed under pressure from the collapse in oil prices and demand. 2020.

- [14] Renewable Energy Focus. Husum Wind 2012: AREVA Wind showcases space-saving Single Blade Installation (SBI) system. 2012.
- [15] Z. Ren, R. Skjetne and Z. Gao. A Crane Overload Protection Controller for Blade Lifting Operation Based on Model Predictive Control. December 2018.
- [16] N. Sharpley. Single blade installation equipment showcased at Husum. 2012.
- [17] Interview with Andries Hofman, GustoMSC, by A.L. Slootweg, 2020.
- [18] A.L. Slootweg. Single blade installation with a floating monohull crane vessel - Determining the optimal installation method. December 2020.
- [19] L. Li, Z. Gao, and T. Moan. Joint Distribution of Environmental Condition at Five European Offshore Sites for Design of Combined Wind and Wave Energy Devices. *Journal of Offshore Mechanics and Arctic Engineering*, 2015.
- [20] K. de Leeuw. Single lift blade alignment for large offshore wind turbines. December 2019.
- [21] Zhiyu Jiang. The impact of a passive tuned mass damper on offshore single-blade installation. *Journal of Wind Engineering and Industrial Aerodynamics*, 2018.
- [22] SeaTools. Standardized ahc hoisting winches.
- [23] Jan-Willem van Wingerden. Stability Margins and MPS - WB3240, 2021.

# A | Vessel and Blade data

## A.1 Vessel data

Table A.1.1: Vessel Properties from WAMIT data (\*:from water line, midship, on the stern)

Property	Abbreviation	Value	Unit
Length on waterline	$L_{wl}$	257	m
Breadth	B	60	m
Draft	T	5.6	m
Waterplane area	$A_{wl}$	8652.5	m <sup>2</sup>
Longitudinal metacentric height	$GM_l$	434	m
Transverse metacentric height	$GM_t$	32.07	m
Displacement	$\Delta$	$4.32 \cdot 10^4$	m <sup>3</sup>
Inertia around x-axis	$I_{xx}$	$3.57 \cdot 10^{10}$	m <sup>4</sup>
Inertia around y-axis	$I_{yy}$	$1.71 \cdot 10^{11}$	m <sup>4</sup>
Inertia around z-axis	$I_{zz}$	$1.60 \cdot 10^{11}$	m <sup>4</sup>
Critical roll damping	$c_{cr,44}$	$4.46 \cdot 10^{10}$	m <sup>4</sup> /s
Crane tip x-coordinate*	$X_{ct}$	52.5	m
Crane tip y-coordinate*	$Y_{ct}$	45	m
Crane tip z-coordinate*	$Z_{ct}$	175	m

## A.2 Blade data

Table A.2.1: Blade properties [11]

Description	Abbreviation	Value	Unit
Length	$L_b$	117	m
Blade mass	$m_b$	65.25	t
Root diameter	$d_r$	5.20	m
Distance CoG to blade root	$l_{br}$	26.8	m
Nacelle and hub mass	$m_{nh}$	822	t
Hub height	$h_{hub}$	150	m
Inertia around z-axis	$I_{b,zz}$	$2.26 \cdot 10^7$	$m^4$
Breadth blade gripper	$l_{bg}$	20	m
Summation of all segment areas times the according coefficient for y-force	$\xi_f$	65.8	$m^2$
Summation of all segment areas times the according coefficient for y-force times the distance to the blade CoG	$\xi_m$	2171.4	$m^2$

### A.3 Blade nodes

Table A.3.1: Nodes of IEA 15MW reference turbine blade [11]

Node	Spanwidth position [r/R]	Chord [m]	Twist [rad]	Node	Spanwidth position [r/R]	Chord [m]	Twist [rad]
1	0.000	5.20	0.272	31	0.618	3.59	0.007
2	0.020	5.21	0.272	32	0.638	3.50	0.003
3	0.040	5.24	0.269	33	0.657	3.42	0.000
4	0.060	5.29	0.262	34	0.676	3.33	-0.004
5	0.080	5.36	0.250	35	0.695	3.24	-0.007
6	0.100	5.44	0.236	36	0.715	3.16	-0.012
7	0.125	5.55	0.215	37	0.734	3.07	-0.017
8	0.150	5.65	0.193	38	0.753	2.98	-0.022
9	0.169	5.71	0.176	39	0.772	2.90	-0.027
10	0.188	5.75	0.161	40	0.800	2.77	-0.034
11	0.207	5.77	0.147	41	0.819	2.68	-0.037
12	0.226	5.76	0.136	42	0.838	2.59	-0.038
13	0.245	5.70	0.125	43	0.856	2.49	-0.038
14	0.266	5.60	0.114	44	0.875	2.40	-0.038
15	0.287	5.46	0.103	45	0.894	2.30	-0.037
16	0.308	5.31	0.092	46	0.913	2.20	-0.036
17	0.329	5.15	0.083	47	0.931	2.09	-0.034
18	0.351	4.99	0.073	48	0.950	1.99	-0.032
19	0.373	4.85	0.065	49	0.975	1.85	-0.027
20	0.395	4.73	0.058	50	0.979	1.83	-0.027
21	0.417	4.60	0.051	51	0.981	1.81	-0.026
22	0.439	4.48	0.045	52	0.983	1.80	-0.026
23	0.459	4.37	0.039	53	0.985	1.78	-0.025
24	0.479	4.27	0.035	54	0.987	1.76	-0.025
25	0.498	4.16	0.030	55	0.989	1.72	-0.024
26	0.518	4.06	0.025	56	0.991	1.67	-0.024
27	0.538	3.96	0.021	57	0.994	1.58	-0.023
28	0.558	3.87	0.017	58	0.996	1.42	-0.023
29	0.578	3.77	0.014	59	0.998	1.10	-0.022
30	0.598	3.68	0.010	60	1.000	0.50	-0.022

## A.4 Blade segments

Table A.4.1: Segments of IEA 15 MW reference turbine blade [11]

Segment	$y_{begin}$	$y_{end}$	Area [m <sup>2</sup> ]	Segment	$y_{begin}$	$y_{end}$	Area [m <sup>2</sup> ]
1	-26.80	-24.46	12.18	31	45.52	47.87	8.34
2	-24.46	-22.12	12.22	32	47.87	50.10	7.72
3	-22.12	-19.78	12.31	33	50.10	52.33	7.53
4	-19.78	-17.44	12.46	34	52.33	54.57	7.33
5	-17.44	-15.10	12.64	35	54.57	56.80	7.14
6	-15.10	-12.18	16.08	36	56.80	59.03	6.95
7	-12.18	-9.25	16.38	37	59.03	61.26	6.76
8	-9.25	-7.02	12.65	38	61.26	63.49	6.56
9	-7.02	-4.80	12.76	39	63.49	66.80	9.37
10	-4.80	-2.57	12.83	40	66.80	68.99	5.98
11	-2.57	-0.34	12.83	41	68.99	71.19	5.78
12	-0.34	1.88	12.76	42	71.19	73.38	5.57
13	1.88	4.33	13.83	43	73.38	75.58	5.37
14	4.33	6.78	13.54	44	75.58	77.77	5.15
15	6.78	9.23	13.18	45	77.77	79.96	4.93
16	9.23	11.67	12.80	46	79.96	82.16	4.71
17	11.67	14.26	13.09	47	82.16	84.35	4.48
18	14.26	16.84	12.70	48	84.35	87.28	5.61
19	16.84	19.42	12.36	49	87.28	87.70	0.78
20	19.42	22.00	12.05	50	87.70	87.95	0.45
21	22.00	24.58	11.73	51	87.95	88.20	0.45
22	24.58	26.89	10.21	52	88.20	88.45	0.45
23	26.89	29.19	9.96	53	88.45	88.70	0.44
24	29.19	31.50	9.71	54	88.70	88.95	0.44
25	31.50	33.80	9.48	55	88.95	89.20	0.42
26	33.80	36.11	9.25	56	89.20	89.45	0.41
27	36.11	38.46	9.21	57	89.45	89.70	0.37
28	38.46	40.81	8.99	58	89.70	89.95	0.31
29	40.81	43.17	8.77	59	89.95	90.20	0.20
30	43.17	45.52	8.55				

## B | EnsysXL drawings



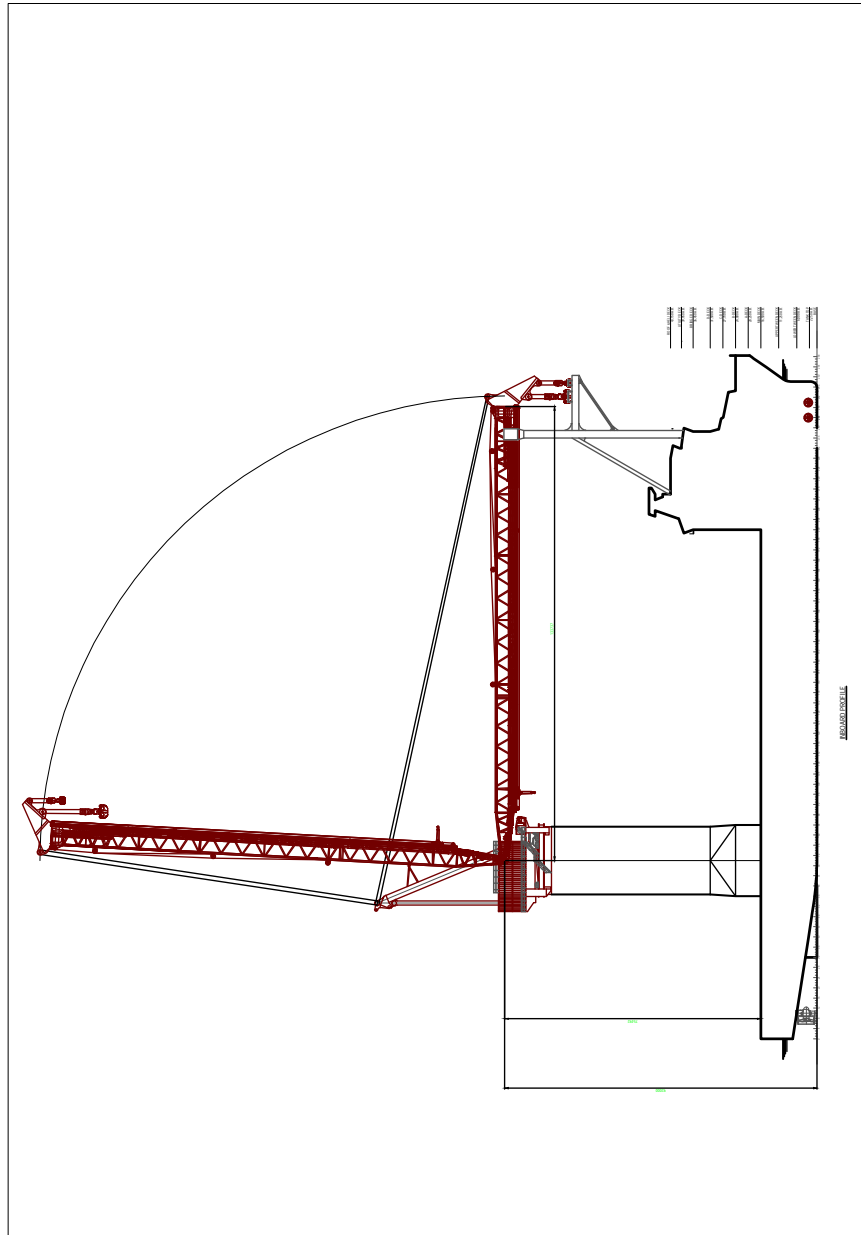


Figure B.0.1: Side view of GustoMSC Ensys XL

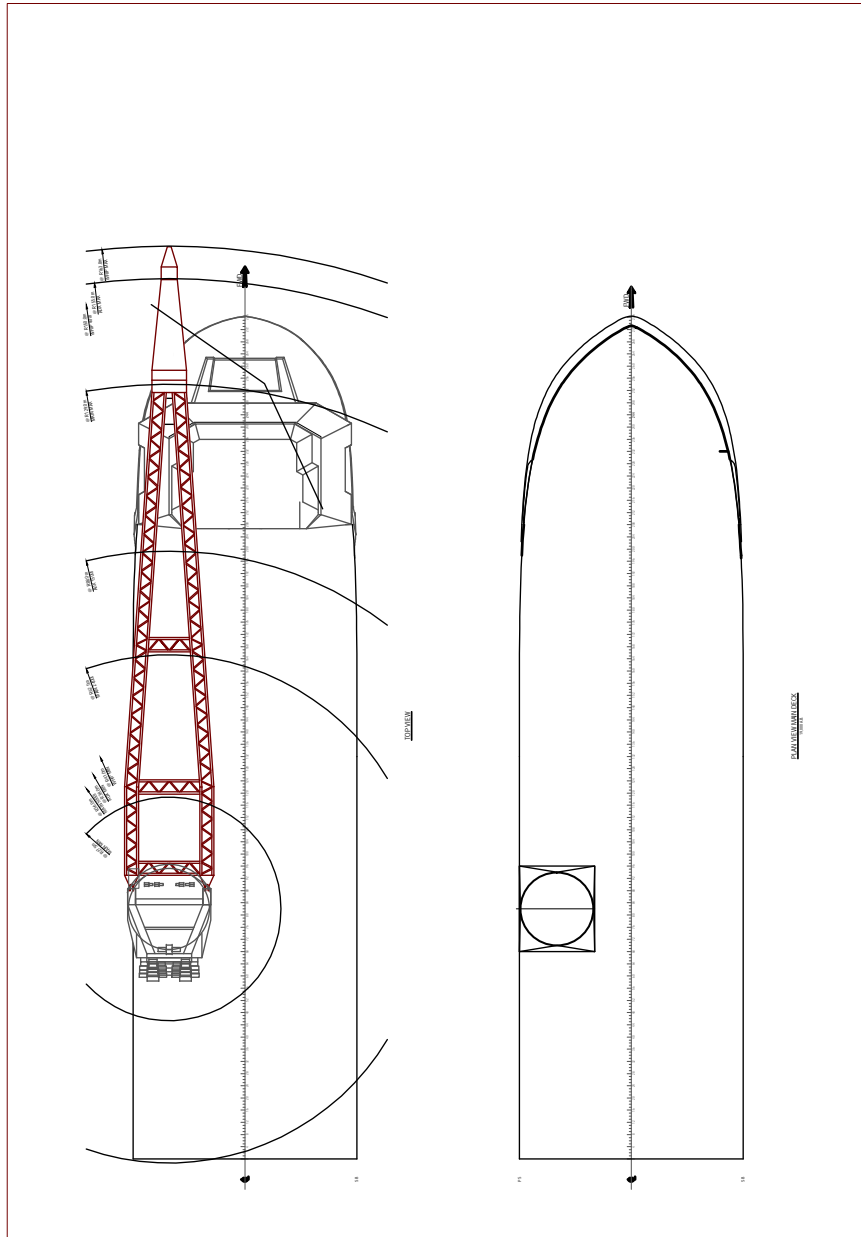
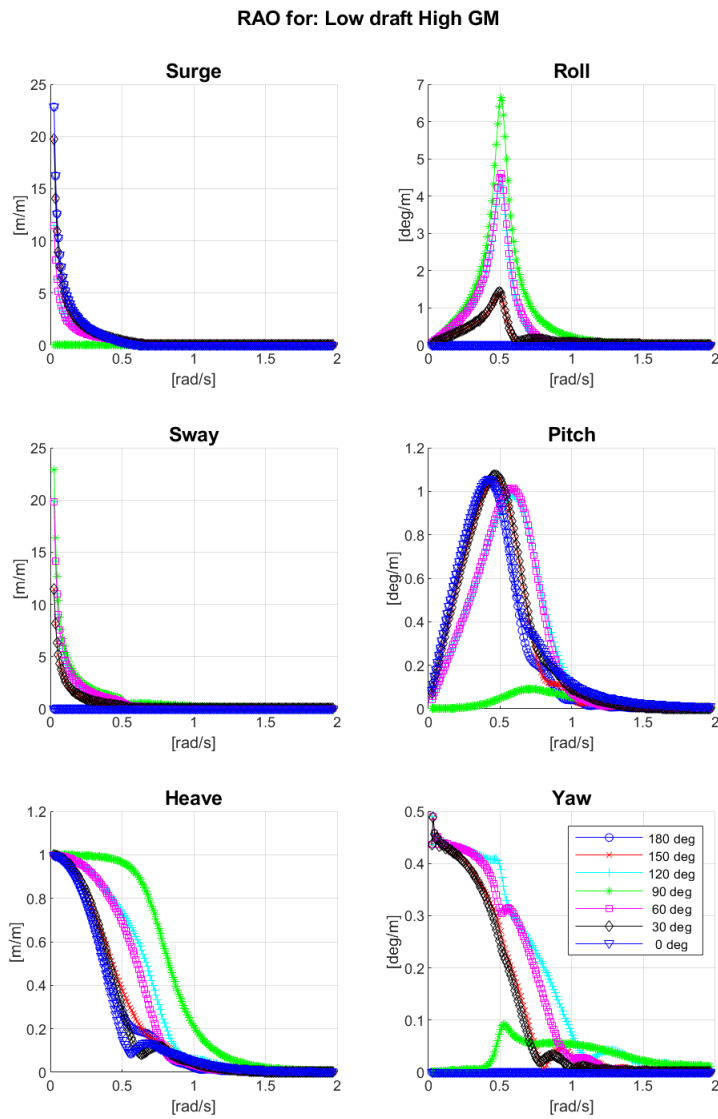


Figure B.0.2: Top view of GustoMSC Ensys XL





# C | RAO - low draft and high GM



ID name :Low draft High GM  
 Plot date :30-Oct-2020 15:40:00  
 Data source:User Defined RAO

Figure C.0.1: RAO for 6 degrees of freedom for a loading condition with a low draft and a high GM

## D | Bode and Nyquist

Bode and Nyquist plots are used during the loop-shaping process to find gain sizes for the controller. The following functions have been plotted for both the  $y$ - and  $\psi$ -compensation controller:

The open loop transfer function  $L(s)$ :

$$L(s) = C(s) \cdot P(s) \tag{D.1}$$

The sensitivity function  $S(s)$ :

$$S(s) = \frac{1}{1 + C(s)P(s)} \tag{D.2}$$

And the closed loop transfer function, or complementary sensitivity function,  $T(s)$ :

$$T(s) = \frac{C(s) \cdot P(s)}{1 + C(s) \cdot P(s)} \tag{D.3}$$

The Nyquist plot gives information about the stability of the system.

In the following sections, the final Bode and Nyquist plots are given for the compensation system in  $y$ - and  $\psi$ -direction.

## D.1 Y-system

In the open loop and sensitivity curve from Figure D.1.1, a peak can be seen at a frequency of 0.62 rad/s. This is the peak for the natural frequency of the plant  $P$ . The peak has been cut-off the graph because it goes to extreme heights. The peak is this large because there is no damping added to the equation. If damping was added, the peak would be less high and the phase step would be more smoothly.

The bandwidth of the system is at 9 rad/s. Since the gain margin is infinitely large, the system does not become unstable when the bandwidth is increased.

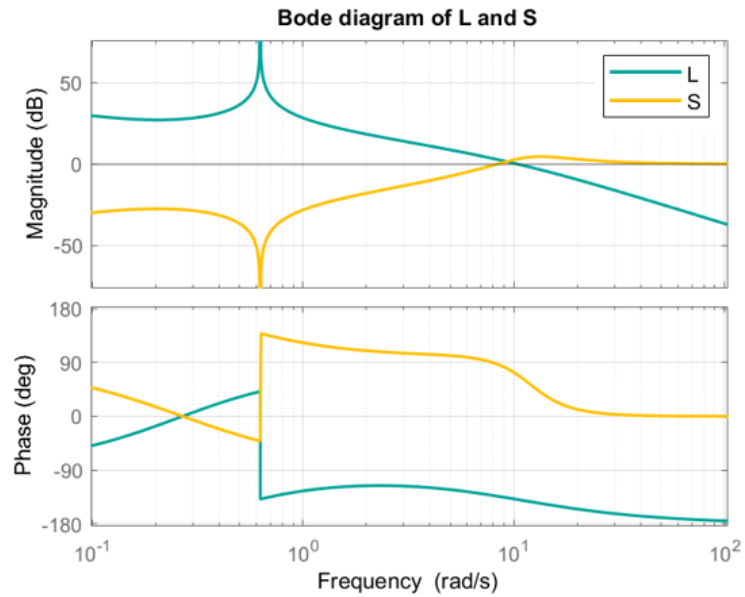


Figure D.1.1: The open loop  $L$  function, and the sensitivity function  $S$  for compensation in y-direction

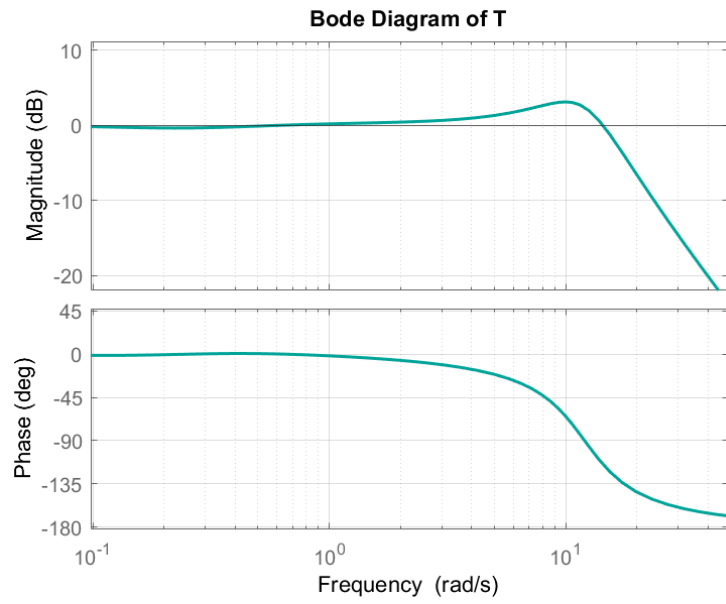


Figure D.1.2: The closed loop function  $T$ , for compensation in y-direction

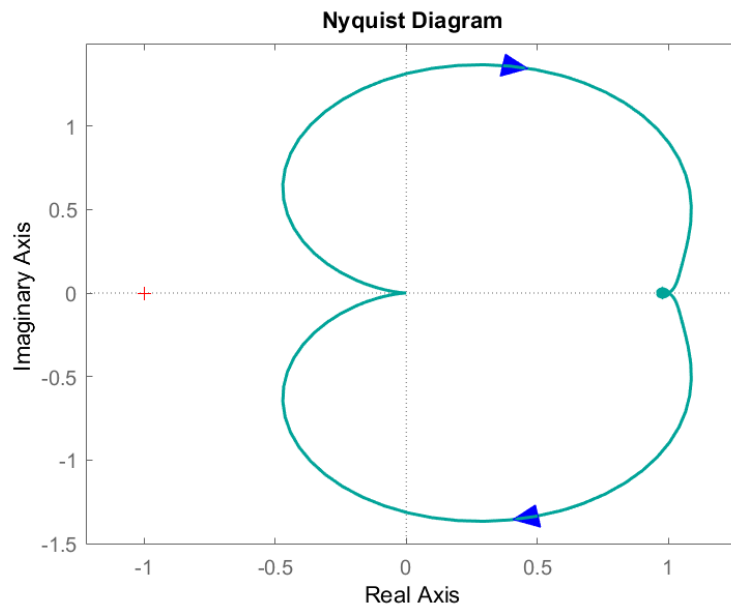


Figure D.1.3: Nyquist plot for  $\psi$ -compensation system



## D.2 $\psi$ -compensation

The natural frequency of  $P_\psi$  is 0 rad/s, as can be seen in Figure D.2.1, the open loop transfer function rises when it comes closer to 0 rad/s. The bandwidth is 22 rad/s, this is a very high frequency, and might give problems with sensors in an actual operation, for now, this is neglected.

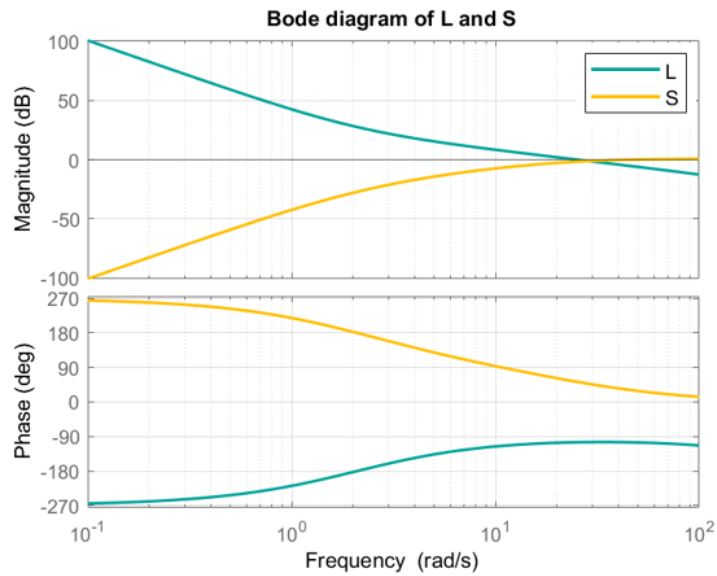


Figure D.2.1: The open loop  $L$  function, and the sensitivity function  $S$  for compensation in  $\psi$ -direction

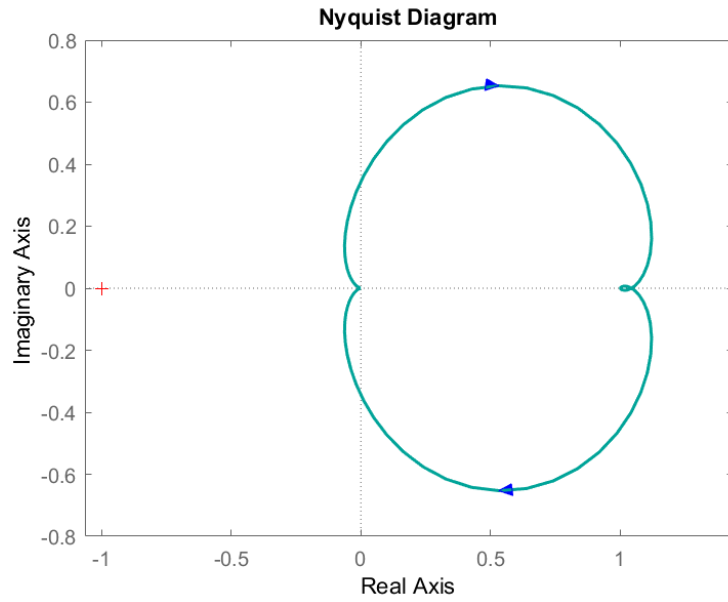


Figure D.2.3: Nyquist plot for  $y$ -compensation system

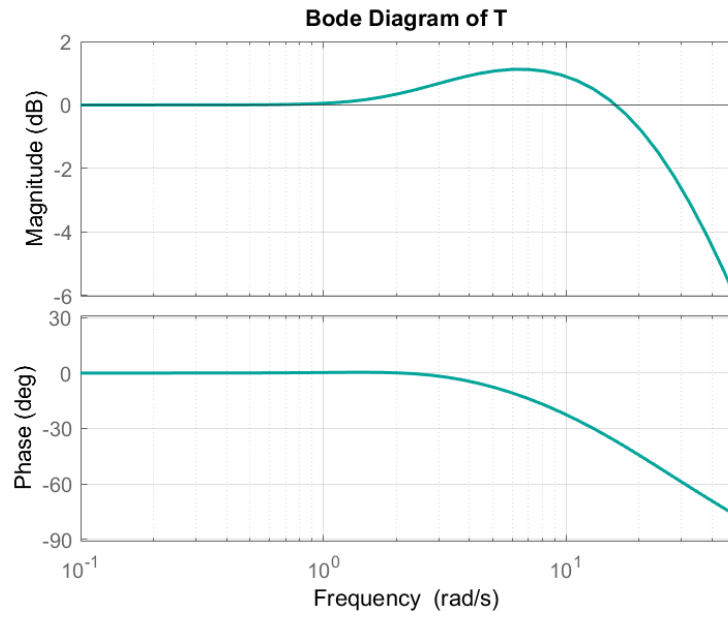


Figure D.2.2: The closed loop function  $T$ , for compensation in  $\psi$ -direction

### D.3 Load sensitivity functions

The last criteria is to lower the disturbance sensitivity function as much as possible. The load sensitivity function is made independent of the blade properties by determining them as followed:

$$G_{du,y} = \frac{P_y(s)}{1 + P_y(s) \cdot C_y(s)} \cdot \frac{mg}{l_c} \quad (D.4)$$

$$G_{du,\psi} = \frac{P_\psi(s)}{1 + P_\psi(s) \cdot C_\psi(s)} \cdot \frac{I_{zz}}{2\pi} \quad (D.5)$$

After completing the loop shaping process, the dimensionless load sensitivity functions look as followed:

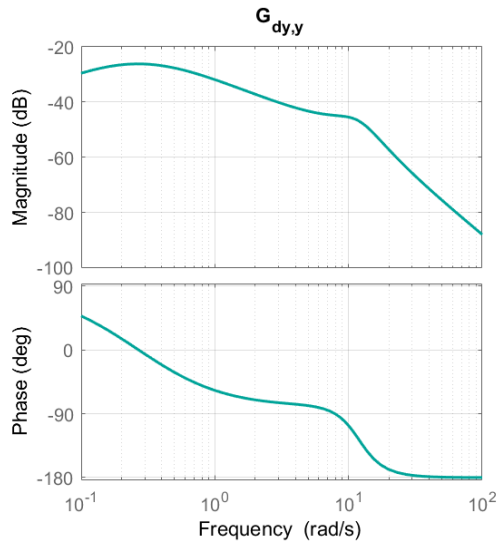


Figure D.3.1: The dimensionless load sensitivity function for y-direction

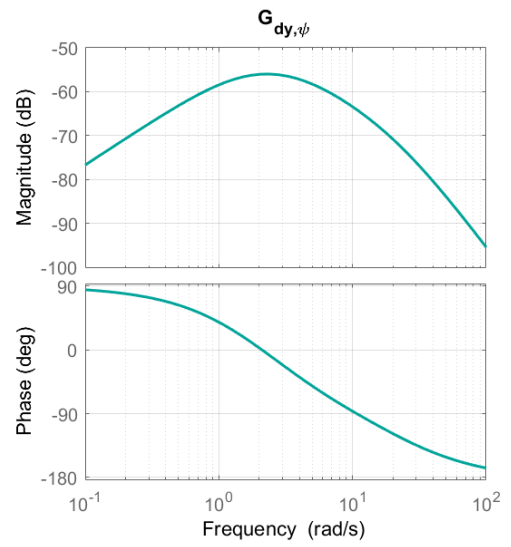


Figure D.3.2: The dimensionless load sensitivity function for  $\psi$ -direction